Sensory experience controls dendritic structure and behavior by distinct pathways involving degenerins

Sharon Inberg and Benjamin Podbilewicz*

Department of Biology, Technion- Israel Institute of Technology, Haifa, Israel

*To whom correspondence should be addressed:

Tel +972 4 8293454 email podbilew@technion.ac.il

Abstract

Tree-like neurites are crucial for receiving information into neurons. It is assumed that nurturing affects the structure and function of dendrites, yet the evidence is scarce, and the mechanisms are unknown. To study whether mechanosensory experience affects dendritic morphology, we use natural mechanical stimulation of the *Caenorhabditis elegans'* polymodal PVD neurons, induced by physical contacts between individuals. We found that animal isolation affects the dendritic tree structure of the PVD. Moreover, developmentally isolated animals show a decrease in their ability to respond to harsh touch. The structural and behavioral plasticity following mechanosensory deprivation are functionally independent of each other and are mediated by an array of evolutionary conserved amiloride-sensitive epithelial sodium channels (degenerins). Our results suggest an activity-dependent homeostatic mechanism for dendritic structural plasticity, acting downstream to mechanosensory activation of degenerins.

Main Text:

The general structure of the nervous system has been known for over a century. Groundbreaking studies on synaptic plasticity and its underlying mechanisms have shown that before birth and in adult animals, brain waves of neural activity are needed for synaptic remodeling [1-4]. In contrast, the molecular mechanisms responsible for structural plasticity of dendritic trees, as an output of different sensory signals, especially during adulthood, are poorly understood [5-7].

43

Figure 1

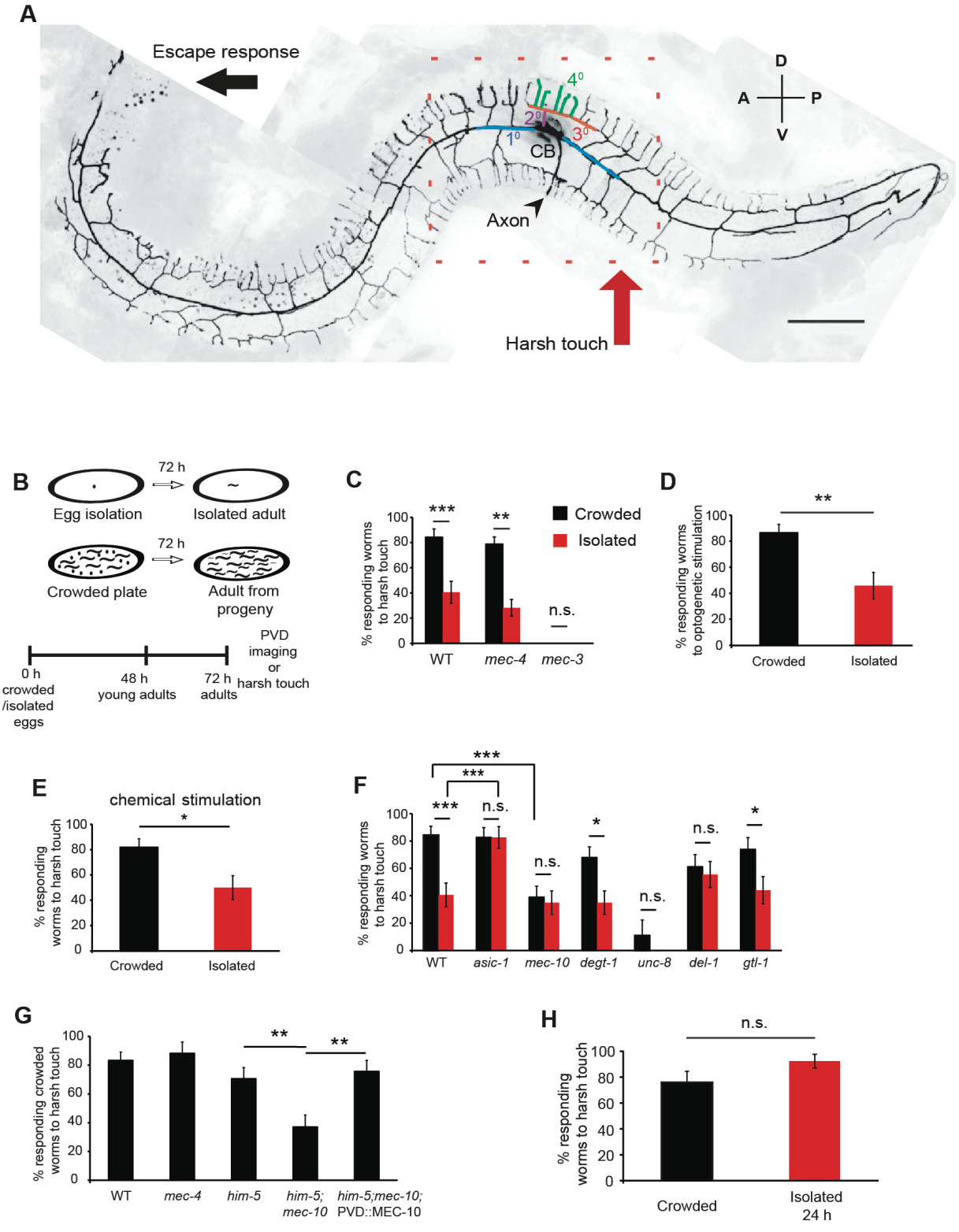

Figure 1. Mechanosensory deprivation during development and cell autonomous activity of MEC-10 reduces the behavioral response of the PVD neuron to activation. (A) Entire branching pattern of the PVD neuron is shown. The red arrow corresponds to the harsh touch contact point with platinum wire, while the left black arrow represents the response of the worm following application of harsh touch. The red dashed square represents the region of interest around the cell body (CB). One representative candelabrum is shown with color coded branch orders. A- anterior; P- posterior; V- ventral; D-dorsal. **(B)** Schematic for the isolation protocol, followed by posterior harsh touch assay or PVD imaging. **(C)** Egg isolation reduced the percentage of responding worms to harsh touch at adulthood. Harsh touch assay was performed for crowded (black bars) and isolated (red bars) worms: Wildtype (WT, N2) worms (Crowded, n=32; Isolated, n=32), *mec-4* (Crowded, n=52; Isolated, n=46. Here the experiment was performed at 96 h since *mec-4* animals develop slower and the worms were L4- young adults at 72 h), *mec-3* (Crowded, n=12; Isolated, n=12). **(D)** Reduced response to photostimulation after isolation. Channelrhodopsin expressing worms on All Trans Retinal were used for analysis of forward escape following photostimulation of the PVD (Crowded, n=30; Isolated, n=24, no response was observed for worms grown without All Trans Retinal). **(E)** Isolation of *mec-4* worms with pheromonal signals resulted in reduced percentage of responding worms (Here the experiment was performed at 96 h since at 72 h the worms were L4s- very young adults; Crowded, n=33; Isolated, n=28). **(F)** DEG-ENaCs and one TRP (*gtl-1*) mutants were tested for the effect of isolation on harsh touch response. Isolated worms were compared to crowded worms from the same strain. WT worms (The same set of worms as in Fig. 1c. Crowded, n=32; Isolated, n=32), *asic-1* (Crowded, n=46; Isolated, n=30), *mec-10* (Crowded, n=38; Isolated, n=31), *degt-1* (Crowded, n=37; Isolated, n=31), *unc-8* (Crowded, n=18; Isolated, n=15), *del-1* (Crowded, n=31; Isolated, n=27), *gtl-1* (Crowded, n=27; Isolated, n=25). **(G)** Strains containing the *ser-2Prom3*::Kaede were tested for their response to harsh touch in the crowded conditions. MEC-10 expression in the PVD rescues the reduction in the response to harsh touch induced by *mec-10* mutants (Crowded: WT, n=42 ;*mec-4,* n=17 ; *him-5,* n=34 (*him-5* was used as WT background for several strains after cross); *him-5;mec-10,* n=35; *him-5;mec-10*;PVD::MEC-10, n=33). **(H)** Isolation of young adult worms for 24 h did not affect the response to harsh touch. Worms were isolated for 24 h as young adults and were tested for harsh touch response, compared to worms that were grown in crowded conditions (Crowded, n=25; Isolated for 24 h, n=26). The proportion of responding worms (percentage) ± standard error of proportion is shown. Fisher exact test, **p*<0.05 ** *p*<0.01, *** *p*<0.001, n.s. not significant.

Mechanistic understanding of experience-dependent dendritic structural plasticity is focused on activity sensation by calcium channels and N-methyl-D-aspartate (NMDA) receptors, that induce downstream signaling cascades including Rho family of small GTPases, calcium metabolism and microtubule stability [8-11]. Since neurological disorders like autism, Down syndrome, fragile X syndrome, and schizophrenia are characterized by abnormal dendritic spine structures, uncovering the molecular basis of dendritic tree instability during development and adulthood, is of great importance [12].

The morphology of the *C. elegans'* PVD bilateral neurons is composed of repetitive and spatially organised structural units that resemble candelabra (Fig. 1A) [13]. These structural properties provide a useful platform to study dendritic morphogenesis. While some of the genetically programmed molecular mechanisms responsible for the development, morphogenesis and regeneration of PVD's dendritic trees are known [14-20], the influence of nurture, e.g. sensory experience, on its structure and function during development and in adulthood remain unexplored. The PVD mediates three sensory modalities: response to harsh touch [21], response to low temperatures [21] and proprioception [22]. Rose et al [23] found that deprivation of mechanosensory stimulation, generated by colliding conspecifics in the growing plate, resulted in reduced response to gentle tap stimulation and modified glutamatergic signalling in gentle touch circuits. Here, we adapted this natural mechanosensory stimulation paradigm to identify the mechanism that couples mechanosensory activity to structural and functional plasticity, focusing on degenerins/epithelial Na^+ channels (DEG/ENaCs) expressed in the PVD [21, 24]. These channels form homo- and hetero-trimers involved in mechanosensation and cognitive functions like learning and memory [25-28]. We investigate how mechanosensory

104 experience, mediated by activity through DEG/ENaCs, affects structural plasticity of the
105 PVD dendritic trees in adult *C. elegans*. Sensory and social isolation affect the behavior
106 and fitness of diverse animals [29], including primates [30]. Our findings on the plasticity of
107 stereotypic dendritic trees of polymodal somatosensory neurons in adult nematodes,
108 reveal mechanisms of dendritic plasticity induced by mechanosensation that may be
109 conserved.

110 **Experience induces behavioral plasticity**

111 To evaluate PVD activity we tested one of its modal functions using a behavioral assay
112 that measures escape from the noxious mechanical stimulus by prodding with a
113 platinum wire (harsh touch assay; Fig. 1A) (*24*). To study whether mechanosensory
114 deprivation affects the nociceptive functions of the PVD [13, 31], we isolated embryos into
115 single plates, from hatching through adulthood and compared their behavioral response
116 to harsh touch against adults that were grown for 72 h on crowded plates (Fig. 1B). We
117 found that ~40% of isolated wildtype (WT) animals responded to harsh touch, compared
118 to ~80% of animals grown in crowded plates (Fig. 1C). To exclude the possibility that
119 gentle touch neurons are involved in this behavioral response, we isolated *mec-4*
120 mutants, which are insensitive to gentle touch [32], and obtained similar results. As a
121 negative control, we used *mec-3* mutants, that are touch insensitive (*31*) and found a
122 similarly low response for both groups (Fig. 1C). Thus, isolation reduces the response to
123 noxious stimuli during adulthood in a process that is independent of gentle touch.

124 To investigate whether the isolation-induced decreased response is a PVD-
125 dependent function, we used optogenetic stimulation [24]. We found that isolation reduced
126 the percentage of worms responding to optogenetic stimulation of the PVD (Fig. 1D),

127 indicating that the plasticity in the response is acting downstream to PVD activation and
128 mechanosensory channels.

129 Since mechanosensory experience can be induced not only by conspecifics
130 present on the plate, but also by solid inert objects [33], we used the *mec-4* strain to
131 compare responses of isolated worms to responses of isolated worms grown in the
132 presence of glass beads. Worms grown in isolation with beads had a similar response
133 compared to animals grown in crowded plates (Fig. S1a). We then used plates pre-
134 stimulated with pheromones (Fig. 1E) and *osm-6* mutants (defective sensory cilia,
135 including the PDE neuron [34] that reduces also harsh touch responses [35] (Fig. S1b)). For
136 both experiments we found that isolation induced a reduction in the response to harsh
137 touch. Thus, behavioral plasticity for harsh touch stimulation of the PVD is dependent
138 on mechanosensory stimulation during development and is chemosensory-independent
139 [35].

140 **MEC-10 affects behavioral plasticity**

141 To study the genetic mechanisms of plasticity during nociceptive response, we
142 performed a candidate gene screen for degenerins (DEG/ENaC) and transient receptor
143 potential (TRP) channels that are expressed in the PVD and affect its behavioral
144 responses [9, 20, 36]. The harsh touch response following isolation was reduced in WT,
145 *degt-1* and *gtl-1* mutants, suggesting that these channels are not directly involved in
146 behavioral plasticity following isolation (Fig. 1F). In contrast, for *del-1*, *asic-1* and *mec-*
147 *10* mutants the difference between isolated and crowded conditions was undetectable,
148 indicating that they are required for behavioral plasticity. Interestingly, while the harsh
149 touch response of *asic-1* mutants was high and similar to crowded WT worms, the

response for *mec-10* mutants was low, similar to isolated WT animals. To test whether the response to harsh touch is dependent on DEG/ENaC activity, we used DEG/ENaC blocker- amiloride for worms that were grown in crowded plates. We found that the response to harsh touch was not affected by continuous growth in the presence of amiloride (Fig. S1C). This result supports the idea that the combinatorial activities of multiple amiloride-sensitive epithelial sodium channels have positive and negative effects on the response to harsh touch (Fig. 1F).

Since MEC-10 is expressed in the PVD and is responsible for its response to harsh touch [21], we asked how it mediates the behavioral plasticity following mechanosensory experience in the crowded, but not isolated conditions. To test whether the activity of MEC-10 is required autonomously in the PVD, we performed a cell-specific rescue experiment, with a plasmid encoding for MEC-10, under a PVD-specific promoter [13, 37]. We found that expression of MEC-10 in the PVD rescues the reduction in response to harsh touch in crowded *mec-10* mutants, indicating that it acts cell autonomously to modulate behavioral plasticity of mechanosensory signals (Fig. 1G) [21].

To determine whether isolation affects the response to harsh touch during development or in adults, we isolated young adults for 24 h and found that isolation of young adults did not affect the response to harsh touch (Fig. 1H). Thus, the isolation-induced reduction in response to harsh touch is MEC-10-dependent and is determined during development.

Figure 2

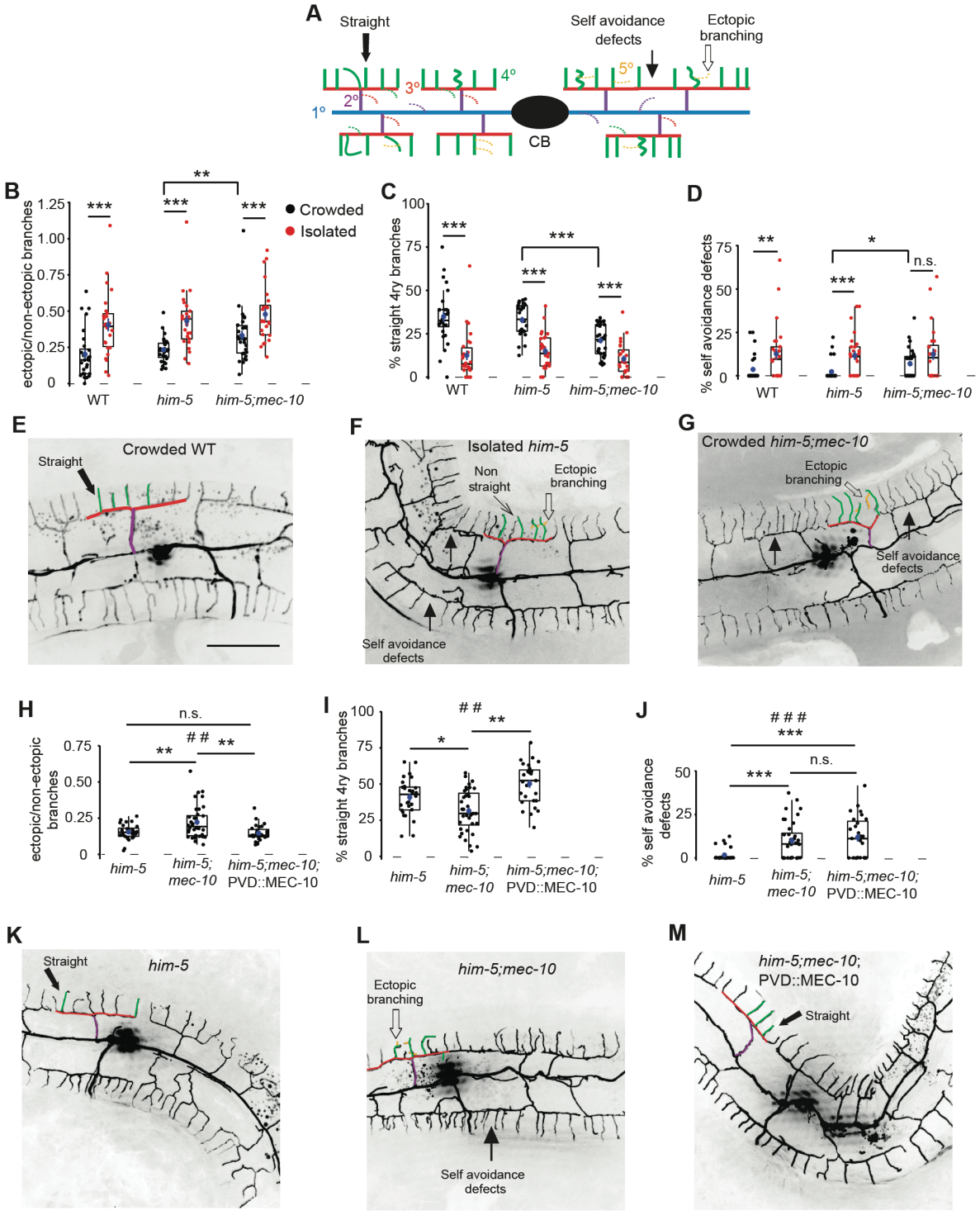

172

Figure 2. Mechanosensory deprivation and cell autonomous activity of MEC-10 affects the architecture of the PVD. (A) Schematic representation for PVD candelabrum structure, with color coded branch orders, ectopic branches, quaternary branching geometry and self-avoidance defects marked and labeled. Dashed lines represent ectopic branching at each order. Isolation and *mec-10* affect the structure of the PVD: **(B)** Increase the fraction of ectopic branching, **(C)** decrease the percentage of straight quaternary branches and **(D)** increase the percentage of self-avoidance defects between two adjacent candelabra were quantified. Crowded (black dots) and isolated (red dots) animals were tested for each strain. WT (Crowded, n=28; Isolated n=26), *him-5* (Crowded, n=27; Isolated, n=25; *him-5* was used as WT background for several strains after cross), *him-5;mec-10* (Crowded, n=30; Isolated, n=24). **(E-G)** Representative pictures from the PVD. Scale bar on panel 'E' represents 50 μm. **(H)** In crowded conditions over- expression of MEC-10 in the PVD, on the background of *him-5;mec-10,* resulted in reduction of ectopic branching and **(I)** increased percentage of straight quaternary branches. **(J)** Over expression of MEC-10 in the PVD does not affect the amount of self-avoidance defects induced by *mec-10.* Crowded *him-5* (n=28), crowded *him-5;mec-10* (n=36), crowded *him-5;mec-10;*PVD::MEC-10 (n=27). **(K-M)** Representative pictures from the PVD. Each dot represents a single worm. The mean ± s.e.m. are shown in blue. Box plot with hinge for the first and third quartile. The median is represented by the thick horizontal black line and the whiskers are estimated calculation of the confidence interval 95%. Kruskal-Wallis test, # # p<0.01, # # # p<0.001, Mann Whitney test with Bonferroni Correction α=0.0167. *p<0.05, ** p<0.01, *** p<0.001, n.s. not significant.

196 **Experience affects morphology via MEC-10**

197 Sensory experience drives synaptic plasticity in the nervous system [3, 4, 38]. To test
198 whether experience regulates the morphology of the dendritic tree of the PVD and its
199 function as a nociceptor [39], we used the mechanical deprivation paradigm (Fig. 1B) and
200 examined morphological features of the PVD (Fig. 2A): **(1)** The fraction of ectopic
201 (excess) out of non-ectopic branches (those that form the classical candelabrum), **(2)**
202 the percentage of straight quaternary branches and **(3)** the percentage of self-
203 avoidance defects between adjacent candelabra.

204 We found that isolation of both WT and *him-5* (the WT background for several
205 strains after cross) animals for 72 h, increased the fraction of ectopic branches
206 compared with age matched crowded worms (Fig 2B), and reduced the percentage of
207 straight quaternary branches (Fig 2C). Moreover, isolation increased self-avoidance
208 defects (Fig. 2D-G, Fig. S2). These results show that the PVD dendritic tree is sensitive
209 to the sensory signals generated by other worms on the plate. Using our quantitative
210 assays to determine changes in the structure of the PVD neuron following
211 mechanosensory isolation, we decided to investigate whether these morphological
212 phenotypes are induced via MEC-10 mechanoreceptor; we compared the PVD
213 arborisation patterns between crowded and isolated *mec-10* mutants. We found that
214 crowded *mec-10* animals were characterized by isolated-like morphological features
215 (more ectopic branches, fewer straight quaternary branches and more self-avoidance
216 defects, compared to crowded *him-5* animals; Fig. 2B-G). These results suggest that
217 PVD morphology is affected by sensory experience in a *mec-10*-dependent pathway. To
218 study whether MEC-10 acts cell autonomously to mediate morphological plasticity, we

used the PVDp::MEC-10 line in a *mec-10* background and found a reduced fraction in the ectopic branches and an increased percentage in the number of straight quaternary branches, compared to age-matched *mec-10* animals (Fig. 2H-I). Interestingly, expression of MEC-10 in the PVD had no effect on the amount of self-avoidance defects (Fig. 2J-M), suggesting that it acts cell non-autonomously to mediate loss of self-avoidance. Activity and sodium influx via the DEG/ENaC UNC-8 promotes synapse elimination in *C. elegans* [40]. To test how global inhibition of DEG/ENaCs affects the morphology of the PVD neuron, we compared crowded worms that were grown on plates with amiloride to control worms. We found that blocking DEG/ENaCs by amiloride increased the fraction of ectopic branching and decreased the percentage of straight quaternary branches, without affecting self-avoidance (Fig. S3). Thus, the structure of the PVD is sensitive to activity and cation influx via DEG/ENaCs. To determine whether the morphological effect on PVD structure is also mediated by mechanical (like friction [41] and collisions [21]), rather than chemical cues, we used glass beads under isolated conditions, to test the effect on the morphology. We found that mechano-stimulation induced by glass beads did not restore the fraction of ectopic branching, but it did significantly increase the number of straight quaternary branches and decreased the percentage of self-avoidance defects (compared with isolated animals without beads, Fig. 3A-E). Thus, mechanosensory stimuli induce morphological plasticity in the PVD via DEG/ENaCs.

Similarly to Fig. 2B-D, animal isolation onto pheromone-conditioned plates [42], increased the fraction of ectopic branching, decreased the percentage of straight quaternary branches and increased the percentage of self-avoidance defects (Fig. S4).

These results indicate that the effect of isolation on the structure of the PVD is not mediated by chemical signals. Additionally, we looked at *mec-4* gentle-touch-insensitive mutants [23, 32] and confirmed that isolation caused a similar change to PVD structure as WT (Fig.S5, compare with Fig. 2B-D). In summary, mechanosensory experience controls morphological plasticity of PVD dendritic trees via MEC-10 activity and independently of MEC-4.

Adult isolation induces tree complexity

Isolation of eggs for 72 h comprises ~48 h of development followed by ~24 h of adulthood. To determine whether the isolation-induced morphological phenotypes of the PVD (Fig. 2A) occur during development or alternatively during adult maintenance, we compared crowded and isolated WT worms after 48 h, as young adults. We found a small but significant difference only for the percentage of straight terminal 4ry branches (Fig. S6), suggesting that isolation affects maintenance of PVD morphology during adulthood. To determine directly the period when mechanical isolation acts to cause structural phenotypes, we studied the morphology of the PVD in worms that were grown in crowded plates and then isolated as young adults for 2, 5 or 24 h. Isolation of adults for 2 h had no significant consequence on the structure of the PVD (Fig. S7A-C), while isolation of adults for 5 h reduced the percentage of quaternary straight branches compared to crowded worms (Fig. S7D-F). In contrast, worms isolated as adults for 24 h (Fig. 3F) showed increased PVD complexity, similar to worms grown under continuous isolation of eggs for 72 h (Fig. 2B-G, Fig. 3G-K). Thus, the architecture of the adult PVD is sensitive to the duration of mechanosensory signals during adulthood.

Figure 3

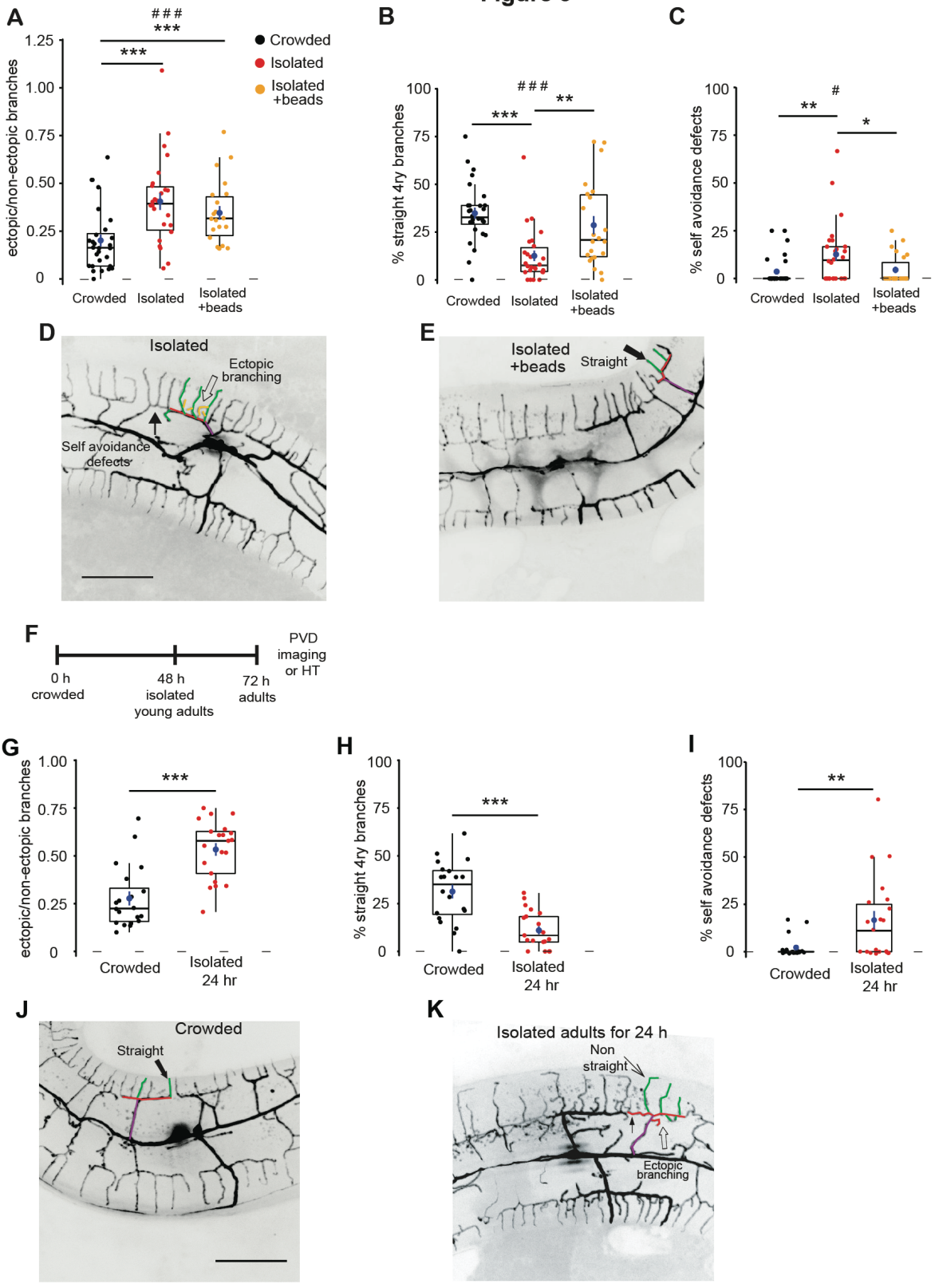

265

Figure 3. The structure of the PVD is plastic during the adult stage and is mechanosensory- and not chemosensory-dependent. **(A)** Egg isolation with glass beads did not affect ectopic branching, but it **(B)** increased the percentage of straight quaternary branches and **(C)** reduced the percentage of self-avoidance defects, compared to isolated worms without beads. **(D, E)** Representative pictures from the PVD for isolated eggs with and without glass beads. Crowded (the same worms as used for Fig. 2B-D), n=28; Isolated (the same worms as used for Fig. 2B-D, n=26); Isolated eggs with beads, n=22. **(F)** Schematic description for the isolation of crowded young adult worms for 24 h, followed by PVD imaging. **(G)** Isolation of young adult worms for 24 h increased the fraction of ectopic branching, **(H)** reduced the percentage of straight quaternary branches and **(i)** increased the percentage of self-avoidance defects (Crowded, n=20; Isolated adults for 24 h, n=21). **(J, K)** Representative pictures from the PVD for crowded and isolated adult for 24 h. Scale bars in panels 'D' and 'J' represent 50 µm. Each dot represents one worm. The mean ± s.e.m. are shown in blue. Box plot with hinge for the first and third quartile. The median is represented by the thick horizontal black line and the whiskers are rough calculation of the confidence interval 95%. Kruskal-Wallis test, # $p<0.05$, # # # $p<0.001$, Mann Whitney test, * $p<0.05$, ** $p<0.01$, *** $p<0.001$, n.s. not significant.

Figure 4

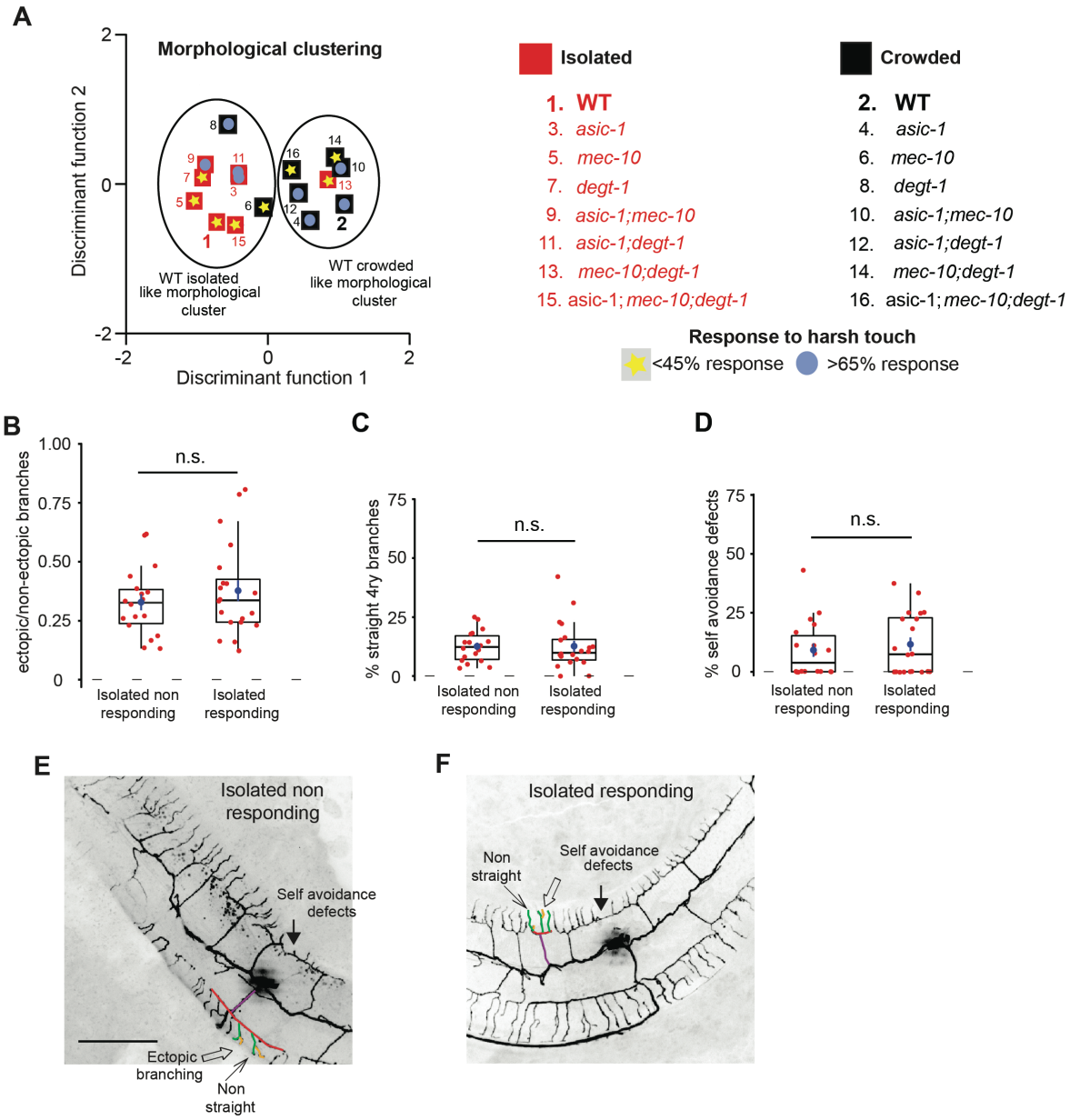

Figure 4. Response to harsh touch and morphology of the PVD are independent

(A) Discriminant analysis revealed the independence of harsh touch on PVD's morphological classification. Worms from a particular treatment (crowded or isolated) and genotype were classified based on their morphological characteristics of the PVD using discriminant analysis and by their response to harsh touch. The squares (black for crowded and red for isolated) are the centroids for the morphological characteristics analyzed in Fig. S9. The response to harsh touch (Fig. S8) is illustrated by its

magnitude (low, <45% in yellow asterisk; high, >65% in light blue circles). The different genotypes (numbers 1-16) are labeled in the list located on the right. Isolated worms were defined based on their response to harsh touch. Isolated harsh touch responding animals were compared to isolated non-responding. No significant difference was measured for **(B**) the fraction of ectopic branching, **(C)** the geometry of quaternary branches or **(D**) the percentage of self-avoidance defects (Isolated non-responding, n=18; Isolated responding, n=20). **(E, F)** Representative pictures from the PVD for responding and non-responding worms. Scale bar for panel 'E' represents 50 µm. The mean ± s.e.m. are shown in blue. Box plot with hinge for the first and third quartile. The median is represented by the thick horizontal black line and the whiskers are rough calculation of the confidence interval 95%. Each dot represents one worm. The mean ± s.e.m. are shown in blue. Mann Whitney test. n.s. not significant.

Structure and function are independent

To test the model proposing that there is a causal link between the morphology of the dendritic tree of the PVD and its function as a nociceptor [39] we followed the isolation protocol described in Fig. 1B for seven combinations of DEG/ENaC mutants and analyzed their response to harsh touch (Fig. S8) and their PVD structure (Fig. S9). To compare the morphological features of different DEG-ENaC genotypes and treatments (crowded, isolated; Fig. S9), we used discriminant analysis as a supervised classification method to combine all the morphological phenotypes analyzed (Fig. 4A). In addition to the data based on morphological similarities between groups, we superimposed the information obtained from behavioral harsh touch experiments for DEG/ENaC mutants (from Fig. S8) on the morphological clustering. We utilized a binary like distribution of the worms in terms of the response to harsh touch (<45% for isolated versus >65% for crowded, as shown in Fig. S8*)*. We found no correlation between the morphology of the PVD and the response to harsh touch when testing the different combinations of genotypes and treatments. In particular, isolated *mec-10;degt-1* mutants show crowded-like morphology with isolated-like behavioral response (Fig. 4A and Fig. S8, S9). These findings suggest that these two proteins are required for the isolation-induced morphological modification of the PVD and represent an example in which the response to harsh touch is independent of the structural alteration of the PVD. Since MEC-10 is important for laminar shear stress [41] and touch [21] we suggest that this channel and its possible partners from the DEG/ENaC family, such as DEGT-1, ASIC-1 and DEL-1 [25, 43, 44], affect the structure and the function of the PVD independently, in an

experience-dependent manner and contrary to the original hypothesis by Hall and Treinin [39].

Additional line of evidence supporting the independence was demonstrated for isolation of young adult worms for 24 h (Fig. 3F). This isolation affects the structure of the PVD (Fig. 3G-K) but has no effect on the response to harsh touch (Fig. 1H). Finally, to directly demonstrate that these two features are independent, we analyzed harsh touch responses of individual animals and then assayed each individual animal for its PVD morphology. We compared the dendritic morphology of individually isolated worms that either responded to harsh touch or didn't. We found that the three morphological parameters were unchanged (Fig. 4B-F). Thus, analysis at the level of individual worms failed to demonstrate a correlation between the morphology and the response to harsh touch. In summary, the morphological and behavioral phenotypes were independently affected by experience via degenerins. We cannot exclude the possibility that other functions of the PVD, like the response to low temperatures [21] and proprioception [22] are more tightly associated to the structure of the PVD.

MEC-10 localization is experience-dependent

Since MEC-10 and DEGT-1 tend to co-localize within the PVD [21] we analyzed the genetic interaction between these two proteins, during mechanosensory experience. Differential localization of degenerins can affect both the behavioral response to harsh touch and also the structural properties of the neuron. We hypothesized that changes in the localization patterns of DEG/ENaC can account for plasticity at both the behavioral (Fig. 1) and the structural level (Figs. 2, 3). MEC-10 localization in the plasma membrane and in intracellular vesicular compartments of the axon and the quaternary

branches was reduced after isolation (Fig. 5A-D, Movies S1 and S2). We also tested the localization pattern of the DEGT-1 [21] in the PVD. In contrast to MEC-10 (Figs. 5A-D), DEGT-1 localization is reduced only in the cell body following isolation (Fig. 5E-H). Furthermore, *degt-1* mutants reduced the amount of MEC-10, and more importantly, abrogated the isolation-induced reduction in MEC-10 localization at the quaternary branches and the axon (Fig. 5A-D). In the reciprocal experiment, DEGT-1 localization at the cell body was affected by *mec-10* mutation, as isolated worms exhibit increased localization compared to WT isolated worms (Fig. 5E-H). Thus, mechanosensory experience induced plasticity in the localization pattern of MEC-10 and DEGT-1. Such experience-dependent plasticity is proposed to be part of the mechanism that locally modulates dendritic and axonal properties, to affect both the structure and the function of the PVD, respectively (Fig. 6).

Figure 5

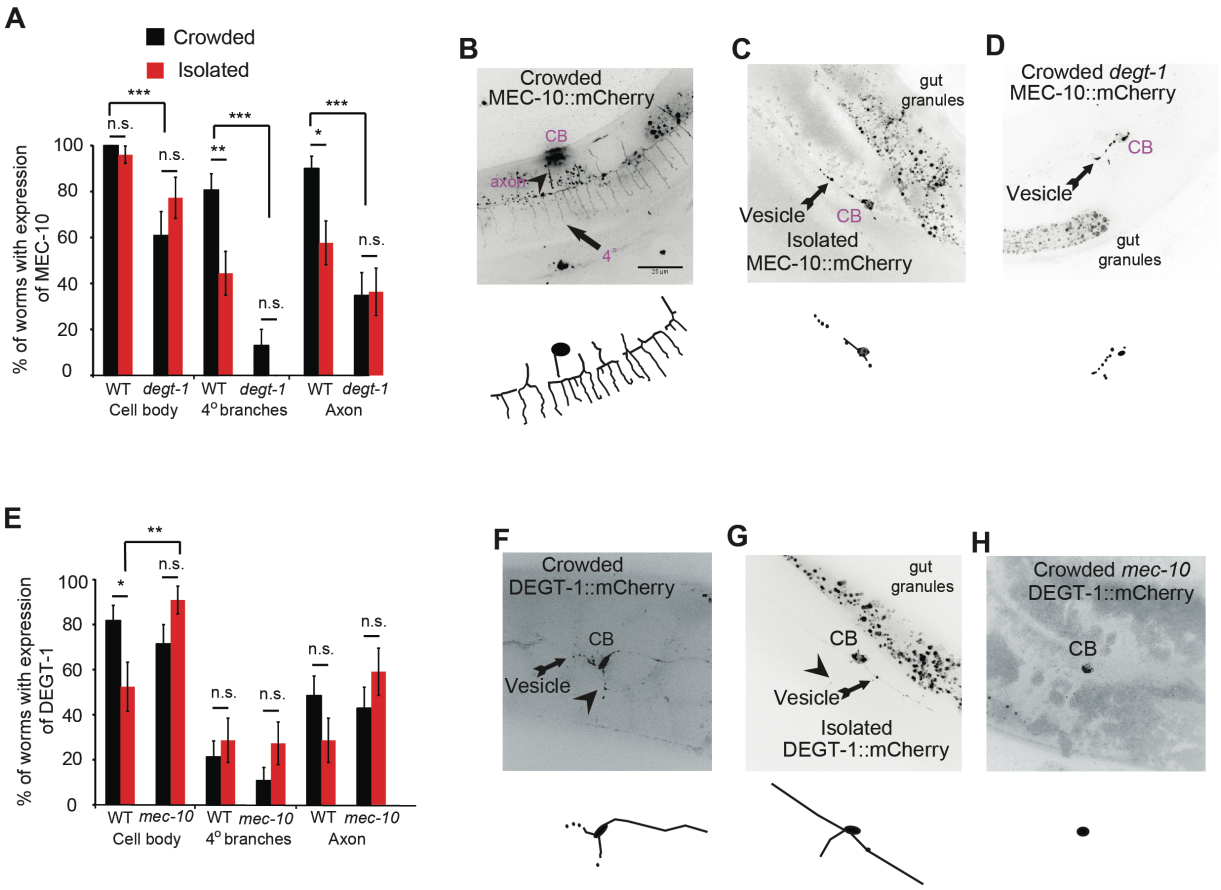

Figure 5. Localization of MEC-10 is mechanosensory- and DEGT-1-dependent. PVD promoter (*ser-2p*) drives the localization of MEC-10::mCherry and DEGT-1::mCherry. Crowded worms were compared to isolated in terms of the localization of MEC-10 and DEGT-1, at three different compartments- the cell body, quaternary branches and axon. **(A)** MEC-10::mCherry localization (shown and labeled in purple) is lower in the quaternary branches and the axon of isolated worms, in a mechanism that is DEGT-1 dependent (WT: Crowded, n=31; Isolated, n=27; *degt-1* mutants: Crowded, n=23; Isolated, n=22). For WT, the same worms as in Fig. 2C were used). **(B, C)** Representative and reconstructions for MEC-10::mCherry localization for crowded and isolated WT worms. Scale bar for panel 'B' represents 50 µm. **(D)** Representative for MEC-10:: mCherry localization for crowded *degt-1* mutants. **(E)** DEGT-1::mCherry localization level is reduced, in MEC-10 dependent-manner, at the cell body, but not in the quaternary branches or the axon of the PVD after isolation, (WT: Crowded, n=33; Isolated, n=21; *mec-10* mutants: Crowded, n=28; Isolated, n=22). **(F, G)** Representative and skeletonized images for DEGT-1::mCherry localization for crowded and isolated worms. **(H)** Representative skeletonized images for DEGT-1::mCherry localization for crowded *mec-10* mutants. The percentage expressing worms ± standard error of proportion is shown. Fisher exact test, *p<0.05, ** p<0.01, *** p<0.01 n.s. not significant.

Figure 6

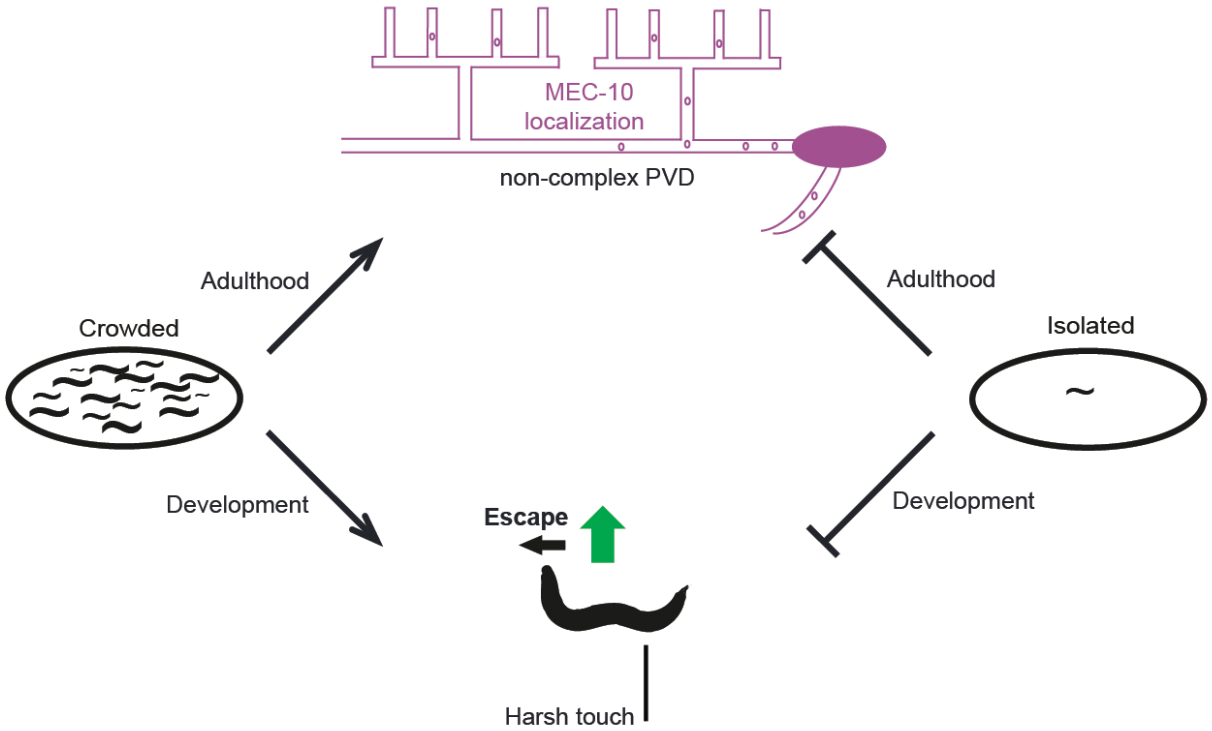

Figure 6. Model of experience-induced plasticity via MEC-10. Mechanosensory experience is a driving force for changes in the localization of MEC-10 in the PVD. Changes in MEC-10 localization (and possibly its partners from the DEG/ENaC family) can induce functional changes in the axon, during development, which in turn may affect the behavioral response to harsh touch. In contrast, changes in localization of MEC-10 (purple) in PVD's dendrites affect the structure of the PVD during adulthood. We propose that the differential spatial and temporal effects of MEC-10 localization are independent. MEC-10 localization in the cell body, axon, dendrites and vesicles is represented in purple and the morphological and behavioral consequences of sensory experience and MEC-10 are illustrated.

Discussion

From the evolutionary point of view, dendritic trees and their structural complexity remain mysterious entities, despite many efforts to understand the contribution of arborization complexity to dendritic physiology [45].

Previous research has demonstrated both cell autonomous [13, 14, 46] and cell non-autonomous [15, 16] mechanisms that regulate PVD's dendritic morphogenesis during development. Few studies have also focused on regeneration and aging effects on the tree structure of the PVD revealing plastic mechanisms during the adult stage [17, 18], similar to what has been shown for *Drosophila* sensory neurons [47]. We have uncovered here that nurture, manifested as mechanosensory experience, activates mechanotransduction signaling, via DEG/ENaCs amiloride-sensitive activity, to maintain the structure of the dendritic tree in adults. Figure 6 shows our working model, where the amount of mechanosensory stimulation, in crowded or isolated conditions, affects the localization of MEC-10 in different compartments of the PVD. Localization of MEC-10, probably by forming high order complexes with other DEG/ENaC, can affect the structure of the PVD at the level of dendritic tree. Thus, experience induced structural plasticity of the dendrites is homeostatic at the dendritic branch level. In contrast, we demonstrate that the response to harsh touch is modulated by the duration and timing of mechanosensory experience and by the presence of degenerins during development. Behavioral plasticity is probably a synaptic property, mediated by DEG/ENaC [48] and related to neurotransmission modulation, independently of the structure of the PVD dendritic tree. These structural and behavioral plasticity are separated in time (adulthood vs. development) and space (dendrite vs. axon).

Somatosensory activation in vertebrates plays a prominent role in shaping the structural and functional properties of dendritic spines, mainly studied in the central nervous system [49-52]. Here we suggest that degenerins mediate mechanosensation-induced dendritic growth in sensory dendrites. In contrast to mammalian cortical neurons, much less is known about their degree of plasticity and the molecular mechanisms utilized during adulthood. We suggest that the dendritic plasticity we described bears resemblance to the activity-dependent effect of glutamatergic signaling and NMDA receptors. Activity via NMDA affects dendritic spines as an upstream mechanism of cell signaling, resulting in structural modifications [53-55]. We propose that degenerins mediate mechanosensory signaling sensation, by activating cationic gradients [56], leading to activation of downstream intracellular signaling pathways [8-11], which in turn enable local, actin-mediated [3, 57, 58] structural plasticity in the PVD dendritic branches. In parallel, it is possible that DEG/ENaCs are also modulating pre/postsynaptic homeostatic signaling in the harsh touch circuit, as has been shown in neuromuscular junctions [59].

Thus, we demonstrated mechanosignaling functions for the combinatorial actions of DEG/ENaCs that act as mediators of experience-induced structural plasticity of sensory dendritic trees.

References

1. Katz, L.C. & Shatz, C.J. Synaptic activity and the construction of cortical circuits. *Science* **274**, 1133-1138 (1996).
2. Goodman, C.S. & Shatz, C.J. Developmental mechanisms that generate precise patterns of neuronal connectivity. *Cell* **72 Suppl**, 77-98 (1993).
3. Zuo, Y., Yang, G., Kwon, E. & Gan, W.B. Long-term sensory deprivation prevents dendritic spine loss in primary somatosensory cortex. *Nature* **436**, 261-265 (2005).

4. Fox, K. & Wong, R.O. A comparison of experience-dependent plasticity in the visual and somatosensory systems. *Neuron* **48**, 465-477 (2005).
5. Tavosanis, G. Dendritic structural plasticity. *Dev Neurobiol* **72**, 73-86 (2012).
6. Kolb, B. & Whishaw, I.Q. Brain plasticity and behavior. *Annu Rev Psychol* **49**, 43-64 (1998).
7. Wong, R.O. & Ghosh, A. Activity-dependent regulation of dendritic growth and patterning. *Nat Rev Neurosci* **3**, 803-812 (2002).
8. Sin, W.C., Haas, K., Ruthazer, E.S. & Cline, H.T. Dendrite growth increased by visual activity requires NMDA receptor and Rho GTPases. *Nature* **419**, 475-480 (2002).
9. Ghiretti, A.E.*, et al.* Rem2 is an activity-dependent negative regulator of dendritic complexity in vivo. *J Neurosci* **34**, 392-407 (2014).
10. Zhou, Z.*, et al.* Brain-specific phosphorylation of MeCP2 regulates activity-dependent Bdnf transcription, dendritic growth, and spine maturation. *Neuron* **52**, 255-269 (2006).
11. Vaillant, A.R.*, et al.* Signaling mechanisms underlying reversible, activity-dependent dendrite formation. *Neuron* **34**, 985-998 (2002).
12. Jan, Y.N. & Jan, L.Y. Branching out: mechanisms of dendritic arborization. *Nat Rev Neurosci* **11**, 316-328 (2010).
13. Oren-Suissa, M., Hall, D.H., Treinin, M., Shemer, G. & Podbilewicz, B. The fusogen EFF-1 controls sculpting of mechanosensory dendrites. *Science* **328**, 1285-1288 (2010).
14. Salzberg, Y., Ramirez-Suarez, N.J. & Bulow, H.E. The proprotein convertase KPC-1/furin controls branching and self-avoidance of sensory dendrites in Caenorhabditis elegans. *PLoS Genet* **10**, e1004657 (2014).
15. Salzberg, Y.*, et al.* Skin-derived cues control arborization of sensory dendrites in Caenorhabditis elegans. *Cell* **155**, 308-320 (2013).
16. Dong, X., Liu, O.W., Howell, A.S. & Shen, K. An extracellular adhesion molecule complex patterns dendritic branching and morphogenesis. *Cell* **155**, 296-307 (2013).
17. Kravtsov, V., Oren-Suissa, M. & Podbilewicz, B. The fusogen AFF-1 can rejuvenate the regenerative potential of adult dendritic trees by self-fusion. *Development* **144**, 2364-2374 (2017).
18. Oren-Suissa, M., Gattegno, T., Kravtsov, V. & Podbilewicz, B. Extrinsic Repair of Injured Dendrites as a Paradigm for Regeneration by Fusion in Caenorhabditis elegans. *Genetics* **206**, 215-230 (2017).
19. Dong, X., Shen, K. & Bulow, H.E. Intrinsic and extrinsic mechanisms of dendritic morphogenesis. *Annu Rev Physiol* **77**, 271-300 (2015).
20. Smith, C.J.*, et al.* Time-lapse imaging and cell-specific expression profiling reveal dynamic branching and molecular determinants of a multi-dendritic nociceptor in C. elegans. *Dev Biol* **345**, 18-33 (2010).
21. Chatzigeorgiou, M.*, et al.* Specific roles for DEG/ENaC and TRP channels in touch and thermosensation in C. elegans nociceptors. *Nat Neurosci* **13**, 861-868 (2010).
22. Albeg, A.*, et al.* C. elegans multi-dendritic sensory neurons: morphology and function. *Mol Cell Neurosci* **46**, 308-317 (2011).
23. Rose, J.K., Sangha, S., Rai, S., Norman, K.R. & Rankin, C.H. Decreased sensory stimulation reduces behavioral responding, retards development, and alters neuronal connectivity in Caenorhabditis elegans. *J Neurosci* **25**, 7159-7168 (2005).
24. Husson, S.J.*, et al.* Optogenetic analysis of a nociceptor neuron and network reveals ion channels acting downstream of primary sensors. *Curr Biol* **22**, 743-752 (2012).
25. Chen, Y., Bharill, S., Isacoff, E.Y. & Chalfie, M. Subunit composition of a DEG/ENaC mechanosensory channel of Caenorhabditis elegans. *Proc Natl Acad Sci U S A* **112**, 11690-11695 (2015).
26. Bianchi, L. & Driscoll, M. Protons at the gate: DEG/ENaC ion channels help us feel and remember. *Neuron* **34**, 337-340 (2002).

27. Welsh, M.J., Price, M.P. & Xie, J. Biochemical basis of touch perception: mechanosensory function of degenerin/epithelial Na+ channels. *J Biol Chem* **277**, 2369-2372 (2002).
28. Gillespie, P.G. & Walker, R.G. Molecular basis of mechanosensory transduction. *Nature* **413**, 194-202 (2001).
29. Bailey, N.W. & Moore, A.J. Evolutionary Consequences of Social Isolation. *Trends Ecol Evol* **33**, 595-607 (2018).
30. Harlow, H.F., Dodsworth, R.O. & Harlow, M.K. Total social isolation in monkeys. *Proc Natl Acad Sci U S A* **54**, 90-97 (1965).
31. Way, J.C. & Chalfie, M. mec-3, a homeobox-containing gene that specifies differentiation of the touch receptor neurons in C. elegans. *Cell* **54**, 5-16 (1988).
32. Suzuki, H.*, et al.* In vivo imaging of C. elegans mechanosensory neurons demonstrates a specific role for the MEC-4 channel in the process of gentle touch sensation. *Neuron* **39**, 1005-1017 (2003).
33. Sawin, E.R., Ranganathan, R. & Horvitz, H.R. C. elegans locomotory rate is modulated by the environment through a dopaminergic pathway and by experience through a serotonergic pathway. *Neuron* **26**, 619-631 (2000).
34. Collet, J., Spike, C.A., Lundquist, E.A., Shaw, J.E. & Herman, R.K. Analysis of osm-6, a gene that affects sensory cilium structure and sensory neuron function in Caenorhabditis elegans. *Genetics* **148**, 187-200 (1998).
35. Li, W., Kang, L., Piggott, B.J., Feng, Z. & Xu, X.Z. The neural circuits and sensory channels mediating harsh touch sensation in Caenorhabditis elegans. *Nat Commun* **2**, 315 (2011).
36. Tavernarakis, N., Shreffler, W., Wang, S. & Driscoll, M. unc-8, a DEG/ENaC family member, encodes a subunit of a candidate mechanically gated channel that modulates C. elegans locomotion. *Neuron* **18**, 107-119 (1997).
37. Tsalik, E.L.*, et al.* LIM homeobox gene-dependent expression of biogenic amine receptors in restricted regions of the C. elegans nervous system. *Dev Biol* **263**, 81-102 (2003).
38. Alvarez, V.A. & Sabatini, B.L. Anatomical and physiological plasticity of dendritic spines. *Annu Rev Neurosci* **30**, 79-97 (2007).
39. Hall, D.H. & Treinin, M. How does morphology relate to function in sensory arbors? *Trends Neurosci* **34**, 443-451 (2011).
40. Miller-Fleming, T.W.*, et al.* The DEG/ENaC cation channel protein UNC-8 drives activity-dependent synapse removal in remodeling GABAergic neurons. *Elife* **5** (2016).
41. Shi, S., Luke, C.J., Miedel, M.T., Silverman, G.A. & Kleyman, T.R. Activation of the Caenorhabditis elegans Degenerin Channel by Shear Stress Requires the MEC-10 Subunit. *J Biol Chem* **291**, 14012-14022 (2016).
42. Maures, T.J.*, et al.* Males shorten the life span of C. elegans hermaphrodites via secreted compounds. *Science* **343**, 541-544 (2014).
43. Ben-Shahar, Y. Sensory functions for degenerin/epithelial sodium channels (DEG/ENaC). *Advances in genetics* **76**, 1-26 (2011).
44. Russell, J., Vidal-Gadea, A.G., Makay, A., Lanam, C. & Pierce-Shimomura, J.T. Humidity sensation requires both mechanosensory and thermosensory pathways in Caenorhabditis elegans. *Proc Natl Acad Sci U S A* **111**, 8269-8274 (2014).
45. Hausser, M. & Mel, B. Dendrites: bug or feature? *Current opinion in neurobiology* **13**, 372-383 (2003).
46. Aguirre-Chen, C., Bulow, H.E. & Kaprielian, Z. C. elegans bicd-1, homolog of the Drosophila dynein accessory factor Bicaudal D, regulates the branching of PVD sensory neuron dendrites. *Development* **138**, 507-518 (2011).
47. DeVault, L.*, et al.* Dendrite regeneration of adult Drosophila sensory neurons diminishes with aging and is inhibited by epidermal-derived matrix metalloproteinase 2. *Genes Dev* **32**, 402-414 (2018).

48. Hill, A.S. & Ben-Shahar, Y. The synaptic action of Degenerin/Epithelial sodium channels. *Channels* (2018).
49. Gyorffy, B.A.*, et al.* Local apoptotic-like mechanisms underlie complement-mediated synaptic pruning. *Proc Natl Acad Sci U S A* **115**, 6303-6308 (2018).
50. Holtmaat, A. & Svoboda, K. Experience-dependent structural synaptic plasticity in the mammalian brain. *Nat Rev Neurosci* **10**, 647-658 (2009).
51. Xu, T.*, et al.* Rapid formation and selective stabilization of synapses for enduring motor memories. *Nature* **462**, 915-919 (2009).
52. Yang, G., Pan, F. & Gan, W.B. Stably maintained dendritic spines are associated with lifelong memories. *Nature* **462**, 920-924 (2009).
53. Star, E.N., Kwiatkowski, D.J. & Murthy, V.N. Rapid turnover of actin in dendritic spines and its regulation by activity. *Nat Neurosci* **5**, 239-246 (2002).
54. Nagerl, U.V., Eberhorn, N., Cambridge, S.B. & Bonhoeffer, T. Bidirectional activity-dependent morphological plasticity in hippocampal neurons. *Neuron* **44**, 759-767 (2004).
55. Zhang, Y., Cudmore, R.H., Lin, D.T., Linden, D.J. & Huganir, R.L. Visualization of NMDA receptor-dependent AMPA receptor synaptic plasticity in vivo. *Nat Neurosci* **18**, 402-407 (2015).
56. Kellenberger, S. & Schild, L. Epithelial sodium channel/degenerin family of ion channels: a variety of functions for a shared structure. *Physiol Rev* **82**, 735-767 (2002).
57. Halpain, S. Avoiding Sibling Conflict: Lessons from Dendrite Self-Avoidance in C. elegans. *Neuron* **98**, 864 (2018).
58. Luo, L. Actin cytoskeleton regulation in neuronal morphogenesis and structural plasticity. *Annu Rev Cell Dev Biol* **18**, 601-635 (2002).
59. Younger, M.A., Muller, M., Tong, A., Pym, E.C. & Davis, G.W. A presynaptic ENaC channel drives homeostatic plasticity. *Neuron* **79**, 1183-1196 (2013).
60. Brenner, S. The genetics of Caenorhabditis elegans. *Genetics* **77**, 71-94 (1974).
61. Kim, E., Sun, L., Gabel, C.V. & Fang-Yen, C. Long-term imaging of Caenorhabditis elegans using nanoparticle-mediated immobilization. *PLoS One* **8**, e53419 (2013).
62. Beanan, M.J. & Strome, S. Characterization of a germ-line proliferation mutation in C. elegans. *Development* **116**, 755-766 (1992).
63. Driscoll, M. & Chalfie, M. The mec-4 gene is a member of a family of Caenorhabditis elegans genes that can mutate to induce neuronal degeneration. *Nature* **349**, 588-593 (1991).
64. Yip, Z.C. & Heiman, M.G. Duplication of a Single Neuron in C. elegans Reveals a Pathway for Dendrite Tiling by Mutual Repulsion. *Cell Rep* **15**, 2109-2117 (2016).

Acknowledgments We thank our lab members for their intellectual and technical support. Yael Iosilevskii, Veronika Kravtsov, Anna Meledin, Meital Oren-Suissa, Tom Shemesh, Shay Stern, Yehuda Salzberg and Alon Zaslaver for critically reading and commenting on the manuscript. Ehud Ahissar, Dan Cassel, Michel Labouesse and Kang Shen for fruitful discussions. William Schafer, Max Heiman and Alexander Gottschalk for plasmids and strains. Some strains were provided by the Caenorhabditis Genetics Center (CGC), which is funded by NIH Office of Research Infrastructure Programs (P40 OD010440). This work was supported by grants from the Israel Science Foundation (442/12 and 257/17), Adelis Fund (2023479), and the Ministry of Science Technology and Space (3-13022).

Author contributions SI and BP conceived and designed the experiments. SI performed the experiments. SI and BP analyzed the data and wrote the paper.

Author information:
Competing interests None
Corresponding author BP podbilew@technion.ac.il

Materials and Methods

Strains

Nematode strains were maintained according to standard protocols [60]. The list of the strains is presented in Supplementary Table 1. Strains of the DEG/ENaCs family obtained from the CGC (JPS282: *asic-1*(*ok415*) I; ZB2551: *mec-10*(*tm1552*) X; VC2633: *degt-1*(*ok3307*) V) were crossed with BP709: IS[hmnEx133](*ser-2Prom3::kaede*). The validation of F2 homozygotes for the DEG/ENaCs (including single, double and triple mutants) was performed by PCR amplification of the deleted region in the genome.

Primers for Multiplex PCR:

asic-1(ok415) I: Forward-1: 5' aactggtgtggccacttcaactttc 3';
Forward-2: 5' aaggtttcagatgatcgcgtagtcaag 3'; Reverse: 5' catttctcttcttccgtcagcgc 3'.
***mec-10(tm1552)* X:** Forward-1: 5' acacggctccttcttgagttccga 3'; Forward-2: 5' attcggtttcctcctcttcttccaatgc 3' ; Reverse: 5' cgtttttttcagcgccctttcctgca 3'
***degt-1(ok3307)* V:** Forward-1: **5'** cgagtagctgattatcaaaaagtcctcga 3';
Forward-2: 5' cggatattccagcattggcgaa 3'; Reverse: 5' ttccccgttgatcttctatgtattaca 3'.

Spinning disk confocal microscopy

Prior to imaging, the worms were placed on an agar pad (10%), mounted on top of a microscope glass slide, with 1µl of polystyrene beads (100 nm diameter, from *Polysciences*, Inc.) for their mechanical immobilization, followed by sealing with a coverslip for complete physical immobilization [61] and taken to imaging:
The PVD neuron was visualized by spinning disk confocal microscope, CSU-X, with Nikon eclipse Ti system and iXon3 camera (ANDOR).
Sequential z-series stacks (0.35 µm) from each worm were taken, with Plan Fluor 40X (NA 1.3). The cell body of the PVD was positioned in the middle of the field and the anterior and posterior branches were revealed. Images were captured with MetaMorph, version 7.8.1.0. Figures were prepared with Adobe Illustrator CS version 11.0.0.

Data analysis

The analysis of the PVD structure was performed for the ~200 µm surrounding the cell body. The pictures in TIFF format were analysed with ImageJ, version 1.48 (NIH). The images were converted to their negative form using the "convert lookup table (LUT)" function in ImageJ.

Maximal intensity projection was used for each PVD image.
Ectopic/excess branching defined as described previously [45]. Briefly, ectopic branches defined as those branches that are not part of a wildtype "ideal" candelabrum (menorah) of a late L4 or young adult and those that sprouted at an incorrect position (non-quaternary terminal ends), as illustrated with dashed lines for ectopic branching in Fig. 2A. The total number of ectopic branching was calculated and presented as a fraction, out of non-ectopic branches.
The geometry of each quaternary branch ("candle") was defined in the following manner: Straight geometry- all the pixels that constitute the branch are positioned on a straight line generated with ImageJ. The width of the line (1 pixel) was constant for the entire sets of experiments. The number of straight quaternary branches were divided by the total quaternary branches for each worm and presented as percentage. The analysis was done only for worms which did not move through the Z stack. Moving worms were excluded from the experiment.

Self-avoidance defects- the number of events where two adjacent candelabra overlapped (no gap formation), was divided by the total number of gaps between the candelabra within the frame (Fig. 2A). The self-avoidance values are presented as percentage.

Behavioral procedures

Harsh touch assay

After 72 h, adult worms (both isolated and those from the crowded plate as described below) were transferred using an eyelash separately to a new agar plate (each worm was transferred to a different plate) with 150 µl of fresh OP50 (about 16 h after seeding), in order to avoid accumulation of OP50 on the edge of the bacterial lawn, which might interfere with harsh touch response measurement. After ~45 minutes in the plate, the worms were prodded with a platinum wire posterior to the vulva, above the interface between worm's body and the agar plate [31]. The number of responses to harsh touch was counted every 10 sec. The non-responding worms were defined after two harsh touch events that were observed sequentially without response. More than one response was considered as responsive animal. The percentage of responding worms was calculated for each genotype and treatment. The experimenter was blind to both the genotype and the treatment- crowded or isolated.

Isolation of embryos

The worm isolation procedure was based on previous work [23] with few modifications, as indicated. Isolated animals were grown on 5 cm agar plate with 150 µl of OP50 *E. coli*, while crowded plate worms were grown on 600-700 µl. Adding sufficient amount of OP50, to avoid starvation of the worms in the crowded plate is important. The embryos

and adult worms were isolated with platinum wire. The plates were sealed with one layer of Parafilm M and placed into a plastic box, at 20 ºC, for the entire experiment. Three experimental groups were used for the 72 h (96 h of experiment was performed only for *mec-4* worms, since they were L4- very young adults at 72 h) isolation experiment: **(1)** Single isolated embryos. **(2)** Crowded worms- the progeny of 30 young, non-starved, adults (approximately, 7,000-9,000 worms in different developmental stages, without approaching starvation). **(3)** Crowded adult worms that were isolated for certain amount of time as adults.
After 48/72/96 h (according to the experiment), age matched worms from each group were transferred to 10% agar pad slides for imaging, as described [23].

Isolation of adults

Isolation for 2 h: Crowded plate - the progeny of 30 adults per plate was used. After ~70 h in the crowded plate the worms were isolated using an eyelash into a new plate, with 150 µl of OP50, for 2 h, followed by imaging of the PVD.

Isolation for 5 h: Crowded plate - the progeny of 30 adults per plate was used. After ~67 h in the crowded plate the worms were isolated using an eyelash into a new plate, with 150 µl of OP50, for 5 h, followed by imaging of the PVD.

Isolation for 24 h: Crowded plate- the progeny of 30 adults per plate was used. After ~48 h in the crowded plate the worms (young adults) were isolated using an eyelash into new plates, with 150 µl of OP50, for 24 h, followed by imaging of the PVD or measurement of harsh touch response. The age of the worms was similar to the worms in experiments of embryo isolation for 72 h experiments (Fig. 1B). The isolated worms were compared to age matched worms from the crowded plate (their original plate).

Optogenetic stimulation

Crowded and isolated worms (ZX819: *lite-1(ce314) X; xIs12[pF49H12.4::ChR2::mCherry; pF49H12.4::GFP*]) were grown on OP50 with 100 µM of All Trans Retinal, in order to have functional channel Rhodopsin [24]. After 72 h the worms were singly mounted with eyelash on a chunk (1cm X 1cm) of agar that was mounted on a microscope glass slide. The agar contained fresh but dry OP50, with 100 µM All Trans Retinal. About 30 minutes following the transfer the worms were tested for the response to light. Worms were stimulated with the spinning disk confocal microscope, CSU-X, with Nikon eclipse Ti system and iXon3 camera (ANDOR), at 488 nm wavelength, with laser intensity of 40% and exposure time of 100 ms, with 10X Plan Fluor (NA 0.3) for ~1 second and the forward acceleration response was measured. The experimenter determined the presence or the absence of forward acceleration response to light activation.

Isolation with chemical stimulation

The *glp-4(bn2)* mutants which are sterile at 25 °C were used (~40 worms for each plate), in order to prepare conditioned/chemically stimulated plates [42] prior to isolation of the ser-2Prom3::Kaede (BP709) strain. The *glp-4* mutants were transferred at early larval stage (L1, L2) to a new agar plate for 96 h at 25 °C. After the removal of the *glp-4* mutants, the embryo isolation procedure was used, as described before at 20 °C.

Isolation with glass beads

Single embryos were isolated to agar plates with 150 µl OP50 and 2.5 g of glass beads (1mm diameter) placed on the 150 µl OP50 lawn in the middle of the plate. The worms were isolated for 72 h and tested for response to harsh touch as described above.

Pharmacology

Amiloride hydrochloride hydrate (Sigma, #A7410) 1M stock solution in DMSO was stored at -20°C. A final concentration of 3 mM amiloride in 0.03 % DMSO was prepared in OP50 bacteria and seeded on NGM plates. 650 µl OP50 were seeded on each plate. As a control, 0.03 % DMSO was added to OP50 bacteria. For each plate (control 0.03% DMSO or 3 mM amiloride) 30 non-starved adult worms were added. After 72 h at 20 °C the progeny of the 30 adults were tested as young adults for their PVD morphology and their response to posterior harsh touch, as described in the previous sections.

Analysis of DEG/ENaCs localization in the PVD

Two DEG/ENaCs proteins, PF49H12.4::MEC-10::mCherry and PF49H12.4::DEGT-1::mCherry (the plasmids were provided by W. Schafer's lab, [21] were analysed for their localization in the PVD, by comparing crowded to isolated worms, in a similar behavioral assay as described in Fig. 1b. The presence of the co-injection marker Punc-122::gfp was a prerequisite for analysis. For each individual worm a stack of images was examined and maximal intensity projection was performed. The images were encoded so the analysis was performed in a blind manner. The cell body of the PVD localized at the center of the region of interest with 60X Apochromat (NA 1.40) and the presence or absence of fluorescent signal was examined in three compartments: The cell body, the quaternary branches and the axon of the PVD. The results are shown as percentage of worms that localize the protein at any compartment.

Rescue strain

Worms from BP1022 (*mec-10(tm1552)* X; Is[*hmn*Ex133](*ser-2Prom3::kaede*); *him-5(e1490)* V) were injected into the gonad with a rescuing plasmid for MEC-10, with a PVD specific promoter (pWRS825: *ser-2Prom3::mec-10* genomic) kindly provided by W. Schafer's lab [21]. The injection mix contained *myo-2::gfp* (20 ng/µl) as a co-transformation marker and pWRS825 (80 ng/µl). For both behavioral and structural characterization the *him-5;mec-10* strains, with and without rescuing plasmid, shared the same crowded plate and were differentiated by the presence or absence of the co-injection marker *myo-2::gfp*.

Statistics

For the morphological characterization of the PVD the results are expressed as means (blue circle) ± standard error of the mean (s.e.m.). In the boxplot (first, third quartiles) the upper whisker extends from the hinge to the highest value that is within 1.5 * IQR (inter-quartile range), the distance between the first and third quartiles. The lower whisker extends from the hinge to the lowest value within 1.5 * IQR of the hinge.
The statistical analyses were performed with SPSS software (IBM, version 20) and "R package". Two-tailed tests were performed for the entire data sets.
Since for many experiments the distribution of the data was not normal, a-parametric tests were used: Mann Whitney test for comparison between independent groups.
Kruskal-Wallis test was used for multiple comparisons for more than two groups.
For proportions (percentage worms) ± standard error of proportion was calculated.
Fisher's exact test was used for analysis of differences in proportions. To estimate the variability in proportion we calculated the Standard Error of Proportion: $\sqrt{\frac{(1-p)\cdot p}{n}}$
The dot plot figures were prepared with "R package", the bar charts with Excel software.

Discriminant analysis

Eight different strains (WT and seven DEG/ENaCs), with two treatments (crowded, isolated worms) for each strain were analyzed for Linear discriminant analysis for morphological characteristics, to evaluate similarity between different strains and treatments. Each worm in the data set was characterized by the three morphological characteristics (the fraction of ectopic branching, the percentage straight quaternary branches and the percentage self-avoidance defects). The centroid for morphological characterization was calculated for each condition and represented in square. Data from independent harsh touch experiments are shown for each group. The analysis was performed using SPSS 20.

Supplementary information

Table S1
Figures S1-S9
Movies S1 and S2

764 **Table S1: List of strains and transgenes used in this work**

Strain	Genotype	Details
N2	Wild-type	[60]
JPS282	*asic-1(ok415)* I; *vxEx282*	From Caenorhabditis Genetics Center (CGC)
SS104	*glp-4*(*bn2*) *I*	CGC [62]
CB1338	*mec-3(e1338) IV*	CGC [31]
MT1085	*unc-8(n491) IV*	CGC [36]
VC2633	*degt-1(ok3307) V*	CGC [21]
DR466	*him-5(e1490) V*	CGC, *him-5* was used as WT background for several strains after cross
NC279	*del-1(ok150) X*	CGC [21]
CB1611	*mec-4(e1611) X*	CGC [63]
ZB2551	*mec-10(tm1552) X*	CGC [21]
JPS478	*asic-1(ok415) I*; *mec-10(tm1552) X*; *vxEx478*	CGC
AQ3272	*ljEx637[PF49H12.4::DEGT-1::mCherry; Punc-122::gfp]*	Kindly provided by W. Schafer [21]
AQ3273	*ljEx638[PF49H12.4::MEC-10::mCherry; Punc-122::gfp]*	Provided by W. Schafer [21]
ZX819	*lite-1(ce314) X*; *zxIs12*[*pF49H12.4::ChR2::mCherry; pF49H12.4::GFP*]	Kindly provided by A. Gottschalk [24]
BP709	*Is*[*hmnEx133*](*ser-2Prom3::kaede*)	Kindly provided by C. Yip and M. Heiman [64]
BP925	*mec-4(e1611) X; Is*[*hmnEx133](ser-2Prom3::kaede*)	Cross [17]
BP1021	*him-5(e1490) V*; *Is*[*hmnEx133*](*ser-2Prom3::kaede*)	Cross: BP709 X DR466
BP1022	*mec-10(tm1552) X*; Is[*hmnEx133*](*ser2Prom3::kaede)*; *him-5(e1490) V*	Cross: BP1021 X JPS478
BP1023	*asic-1(ok415) I*; *him-5(e1490) V; Is[hmnEx133](ser-2Prom3::kaede)*	Cross: BP1021 X JPS478
BP1024	*asic-1(ok415) I; mec-10(tm1552) X*; *him-5(e1490) V Is*[*hmnEx133*](*ser-2Prom3::kaede)*	Cross: BP1021 X JPS478
BP1025	*asic-1(ok415) I; degt-1 (ok3307) V*; *mec-10(tm1552) X*	Cross: BP1024 X VC2633
BP1026	*degt-1(ok3307) V; mec-10(tm1552) X*	Cross: BP1024 X VC2633
BP1027	*degt-1(ok3307)* V; *Is*[*hmnEx133*](*ser-2Prom3::kaede)*	Cross: BP1021 X VC2633
BP1028	*asic-1(ok415) I; degt-1(ok3307) V; Is*[*hmnEx133*](*ser-2Prom3::kaede)*	Cross: BP1025 X BP1027
BP1029	*mec-10(tm1552); degt-1(ok3307) V; Is*[*hmnEx133*](*ser-2Prom3::kaede)*	Cross: BP1025 X BP1027
BP1030	*asic-1(ok415) I; mec-10(tm1552) X; degt-1* (*ok3307) V*; *Is*[*hmnEx133*](*ser-2Prom3::kaede)*	Cross: BP1025 X BP1027
BP1031	*degt-1(ok3307) V*; *ljEx638[PF49H12.4::MEC-10::mCherry; Punc-122::gfp*]	Cross: VC2633 X AQ3273
BP1033	*mec-10(tm1552) X*; ljEx637[*PF49H12.4::DEGT-1::mCherry; Punc-122::gfp*]	Cross: BP1022 X AQ3272
BP1034	*mec-10(tm1552) X*; *IS[hmnEx133](ser-2Prom3::kaede); him-5(e1490) V; pWRS825 Ex[ser-2Prom3::MEC-10genomic*]	pWRS825 plasmid provided by W. Schafer [21] was injected into BP1022

765

Supplementary figures

Supplementary Figure 1

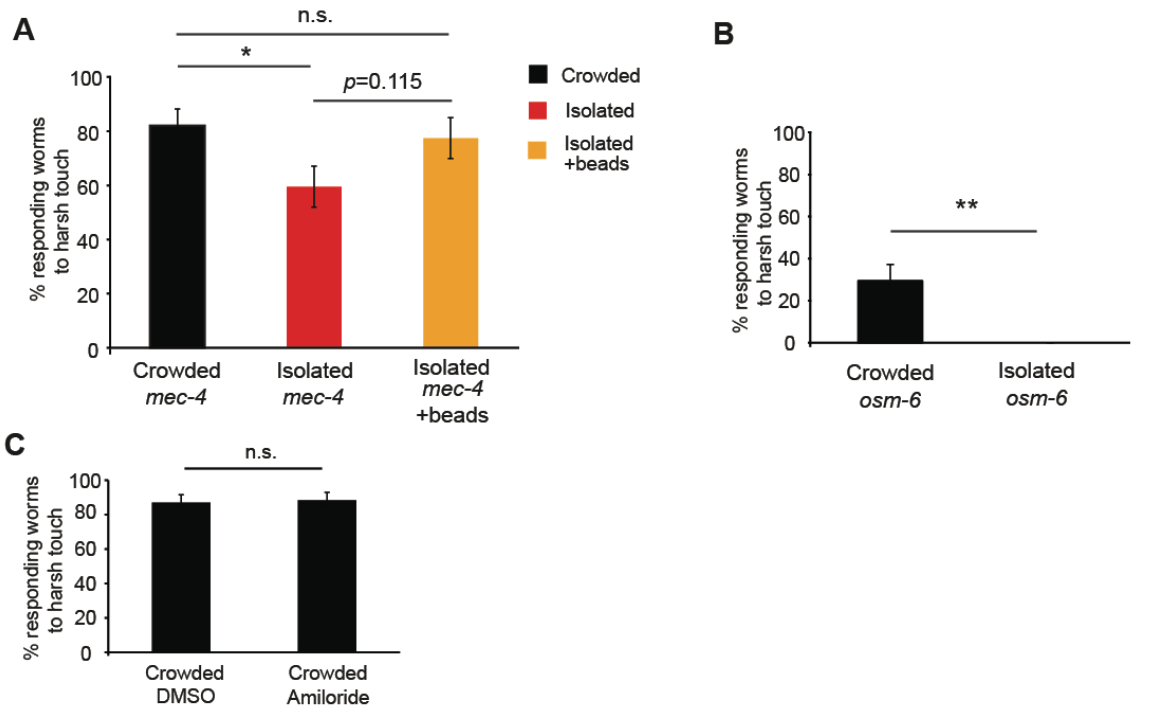

Supplementary Figure 1: The reduction in response to harsh touch following isolation is PVD-dependent and chemosensory-independent. (A) Isolation of gentle touch insensitive *mec-4* worms with glass beads resulted in non-significant increase in the percentage of responding worms, compared to isolated without beads and non-significant difference compared to crowded worms (This experiment was performed at 96 h since *mec-4* animals develop slower and the worms were L4- young adults at 72 h. Crowded, n=39; Isolated, n=42; Isolated egg with beads, n=31). **(B)** Isolation of *osm-6* mutants (impaired in their ciliated neurons, including the PDE which mediates response to harsh touch) resulted in reduced response to harsh touch, when compared to worms from a crowded plate. (Crowded, n=34; Isolated, n=27). **(C)** Continuous exposure to amiloride does not affect the response to harsh touch in the crowded conditions (Crowded DMSO, n=54; Crowded 3 mM amiloride, n=52). The proportion of responding worms (percentage) ± the standard error of proportion is shown. Fisher exact test, * $p<0.05$, ** $p<0.01$, n.s. not significant.

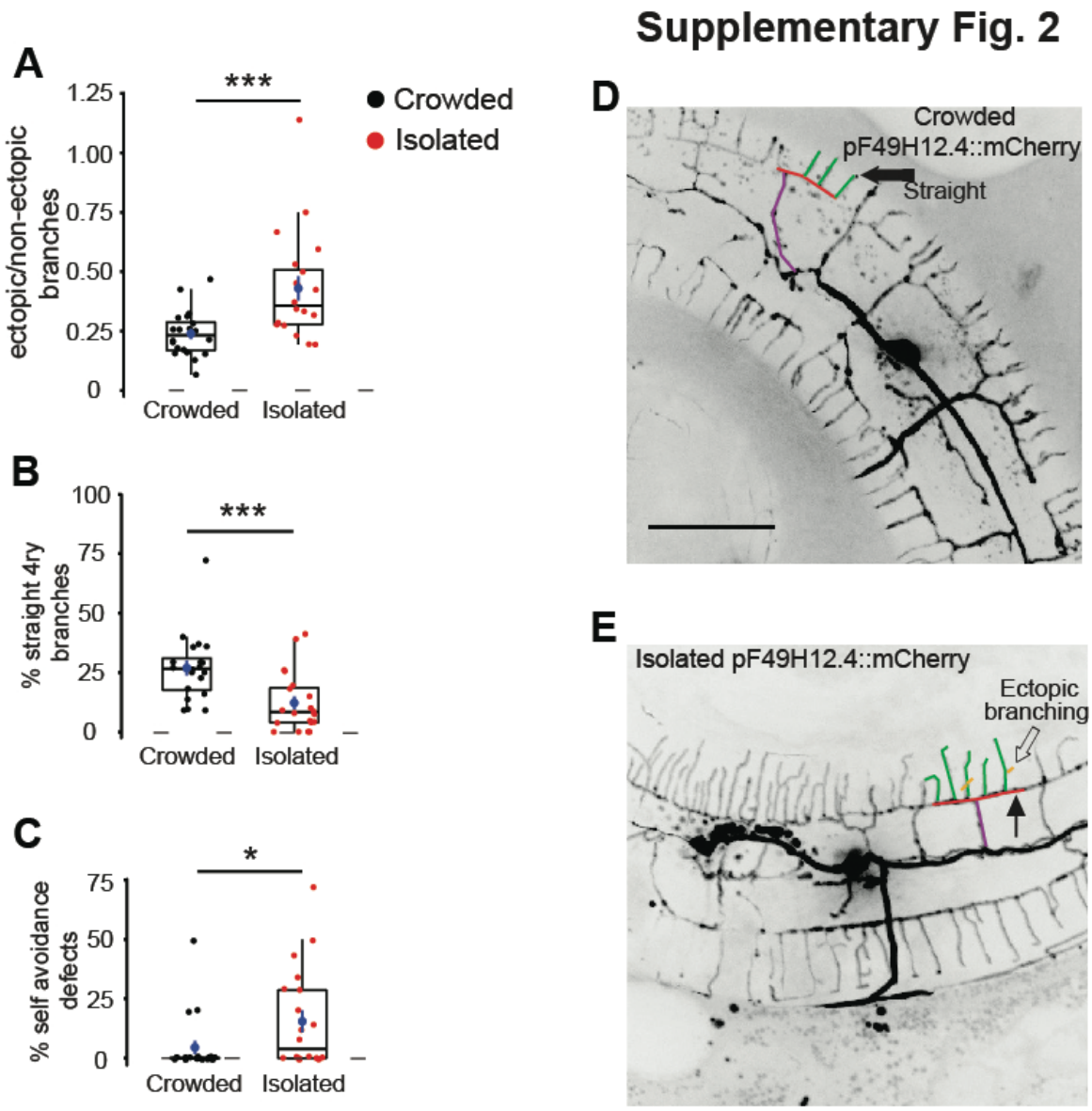

Supplementary Figure 2: The effect of isolation on the structure of the PVD is independent from the identity of the promoter driving expression of the reporter in the PVD. Worms from a different strain and fluorescent marker, F49H12.4::mCherry, were isolated as eggs for 72 h and compared to crowded worms from the same strain. **(A)** Egg isolation for 72 h increased total ectopic branching, **(B)** reduced the percentage of straight quaternary branches and **(C)** increased the percentage of self-avoidance defects between two adjacent candelabra (Crowded, n=20; Isolated, n=20). **(D, E)** Representative pictures from the PVD for crowded worms and isolated eggs. Scale bar for panel 'D' represents 50 µm. The mean ± s.e.m. are shown in blue. Box plot with hinge for the first and third quartile. The median is represented by the thick horizontal black line and the whiskers are estimated calculation of the confidence interval 95%. Mann Whitney test, * $p<0.05$, *** $p<0.001$.

Supplementary Figure 3

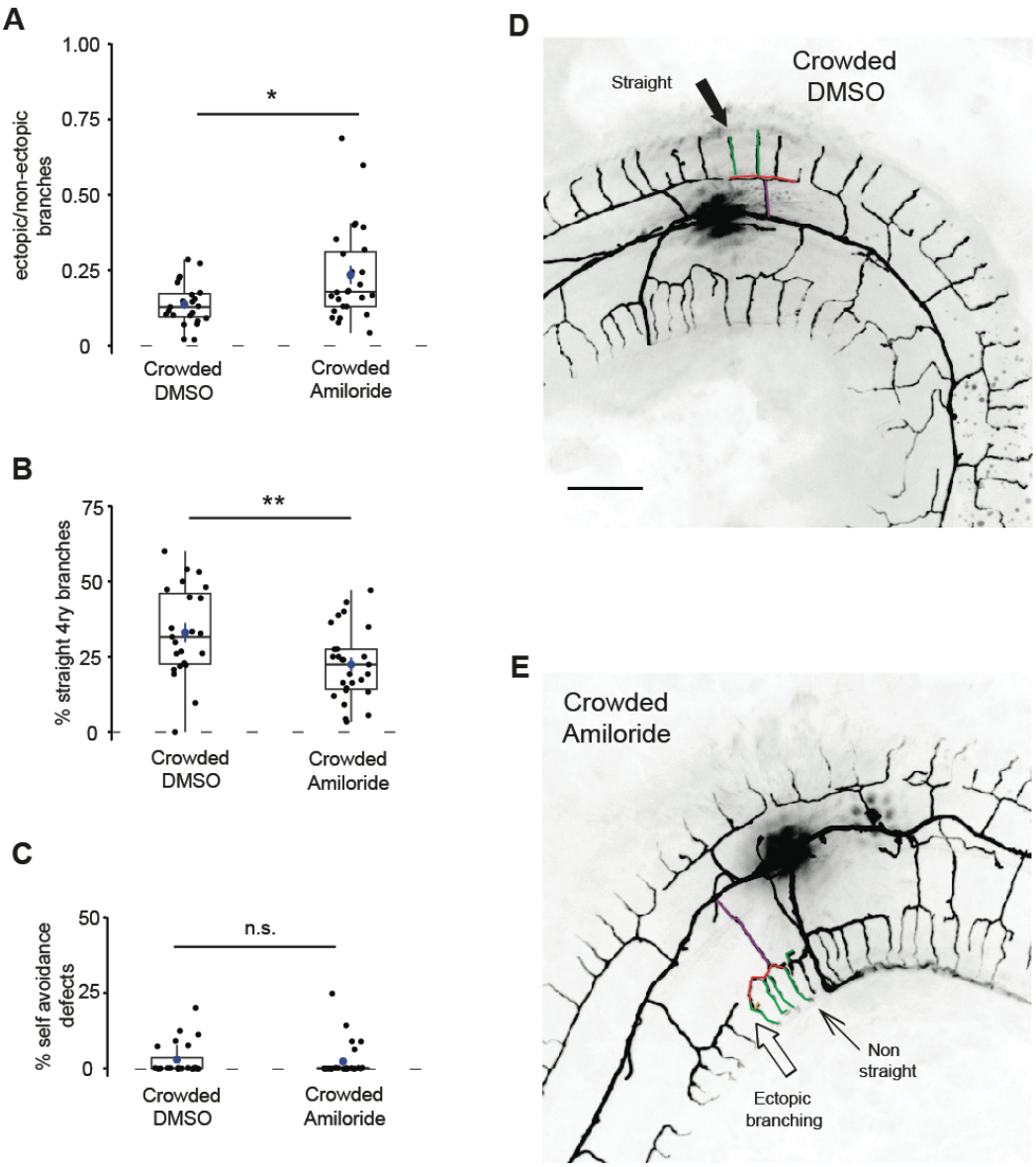

794

795 **Supplementary Figure 3: Blocking DEG/ENaC with amiloride affects the structure**
796 **of the PVD.** Crowded worms that were exposed to 3 mM amiloride **(A)** increased the
797 fraction of ectopic branches, **(B)** decreased the percentage of straight quaternary
798 branches, **(C)** without affecting the percentage of self-avoidance defects (Crowded
799 DMSO, n=23; Crowded 3 mM amiloride, n=27). **(D, E)** Representative images from the
800 PVD for DMSO and amiloride treated worms. Scale bar for panel 'D' represents 50 µm.
801 The mean ± s.e.m. are shown in blue. Box plot with hinge for the first and third quartile.
802 The median is represented by the thick horizontal black line and the whiskers are
803 estimated calculation of the confidence interval 95%. Mann Whitney test *p<0.05, **
804 p<0.01, n.s. not significant.

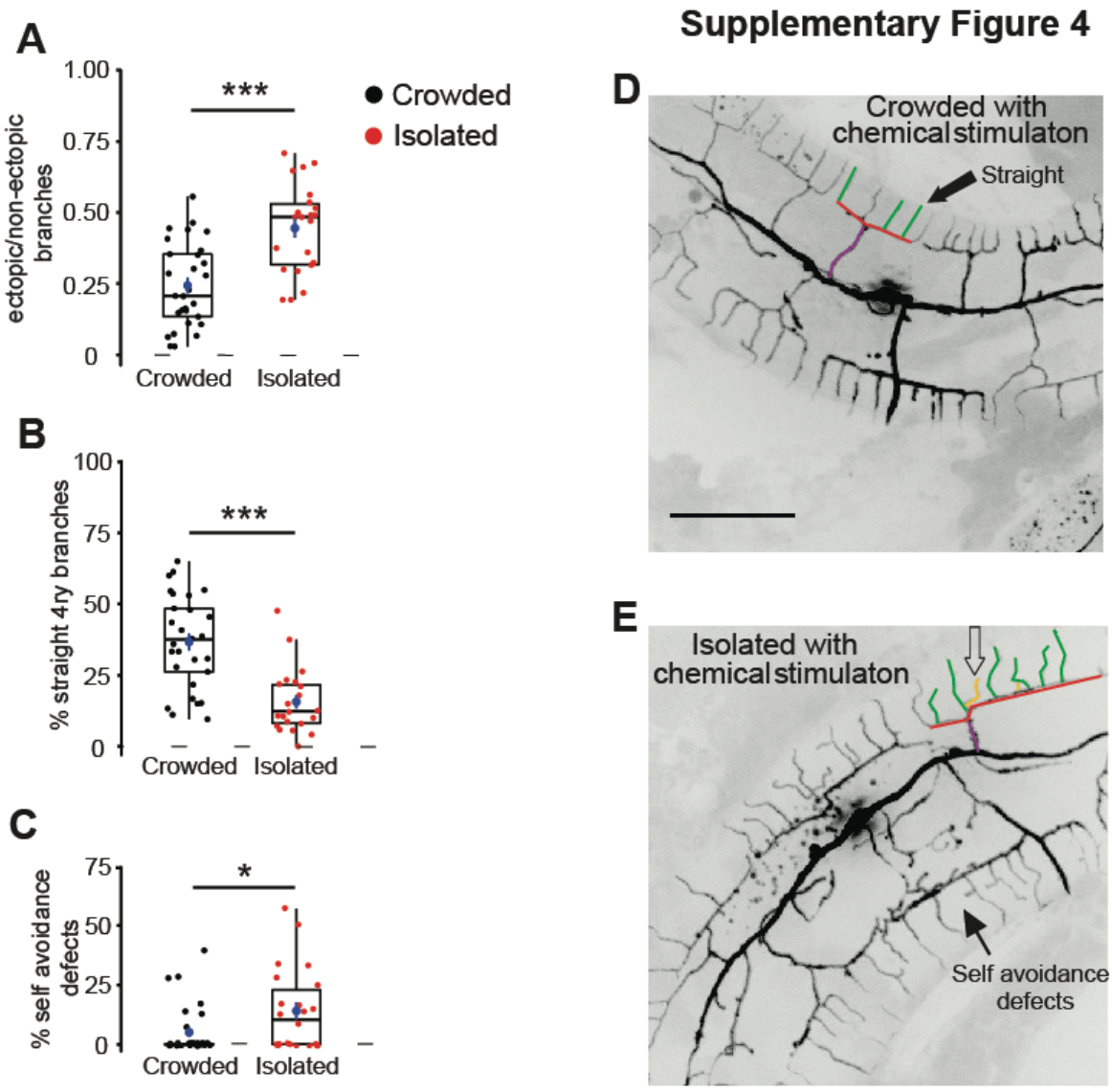

Supplementary Figure 4: The PVD undergoes isolation-dependent structural plasticity in the presence of pheromonal signals in the plate. Both crowded and isolated worms were pre-exposed to pheromonal signals, released by *glp-4* worms (~40 worms for 96 h. The *glp-4* worms were taken out of the plate and the isolation protocol described in Fig. 1b was used). **(A)** Chemical stimulation of plates with *glp-4*, followed by egg isolation, increased the fraction of ectopic branching, **(B)** decreased straight quaternary branches and **(C)** increased the percentage of self-avoidance defects (Crowded, n=24; Isolated, n=20). **(D, E)** Representative pictures from the PVD for crowded and isolated worms with chemical stimulation of the plates. Scale bar for panel 'D' represents 50 µm. The mean ± s.e.m. are shown in blue. Box plot with hinge for the first and third quartile. The median is represented by the thick horizontal black line and the whiskers are estimated calculation of the confidence interval 95%. Mann Whitney test, * $p<0.05$, *** $p<0.001$.

Supplementary Figure 5

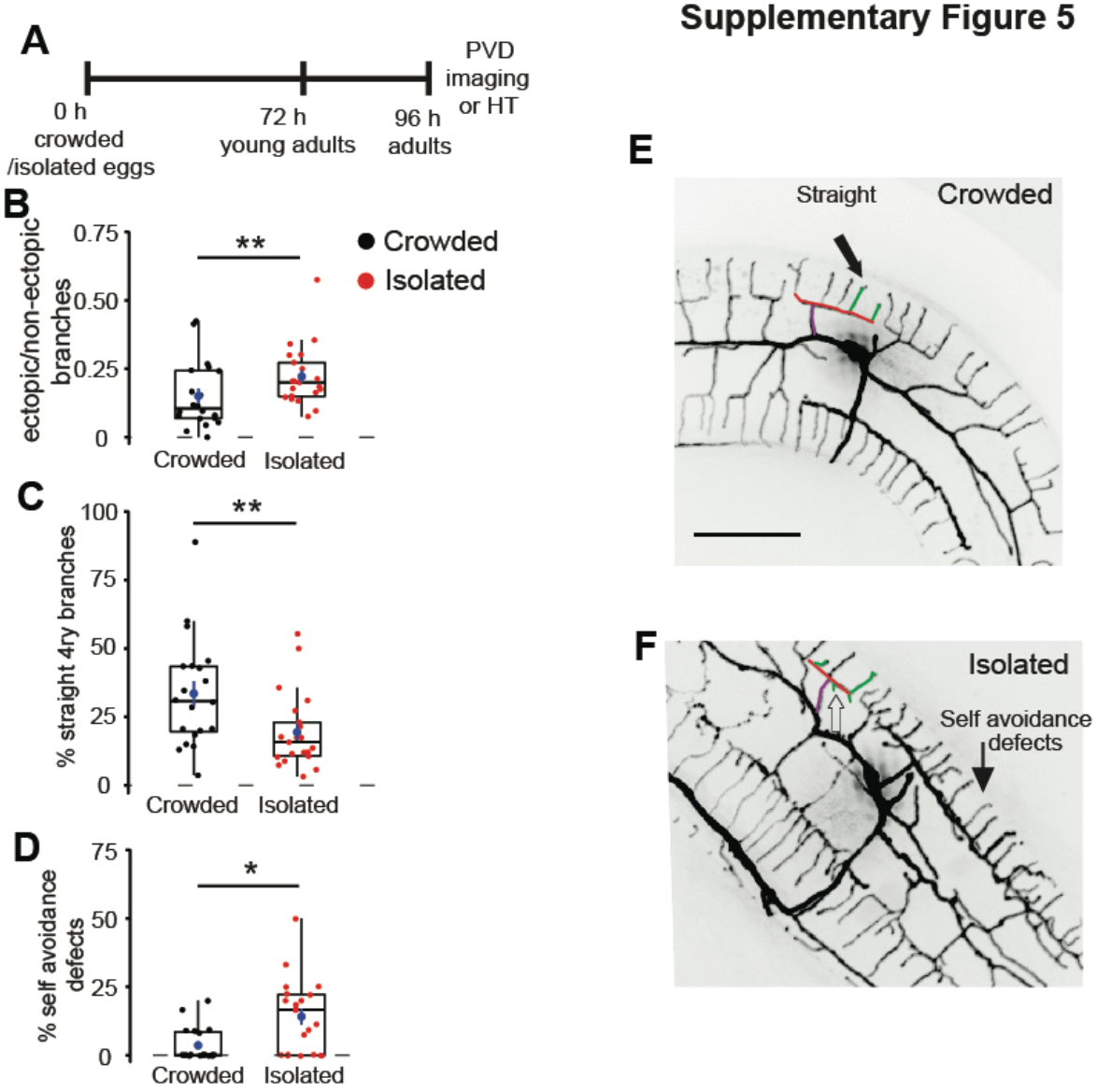

Supplementary Figure 5: The effect of isolation on the structure of PVD is not mediated by the gentle touch mechano-sensory neurons. (A) Description of the protocol for the isolation of *mec-4* eggs for 96 h (the experiment was performed for 96 h since the worms were L4s or very young adults at 72 h), followed by PVD imaging. **(B)** Isolation of the gentle touch impaired strain, *ser-2Prom3*::Kaede;*mec-4*, increased total ectopic branching, **(C)** reduced the percentage of straight quaternary branching and **(d)** increased the percentage of self-avoidance defects after isolation of eggs. Crowded, n=20; Isolated, n=21. **(E, F)** Representative pictures from the PVD for crowded worms and isolated eggs. Scale bar panel on 'E' represents 50 µm. The mean ± s.e.m. are shown in blue. Box plot with hinge for the first and third quartile. The median is represented by the thick horizontal black line and the whiskers are estimated calculation of the confidence interval 95%. Mann Whitney test with Bonferroni correction α=0.0167, * p<0.05, ** p<0.01.

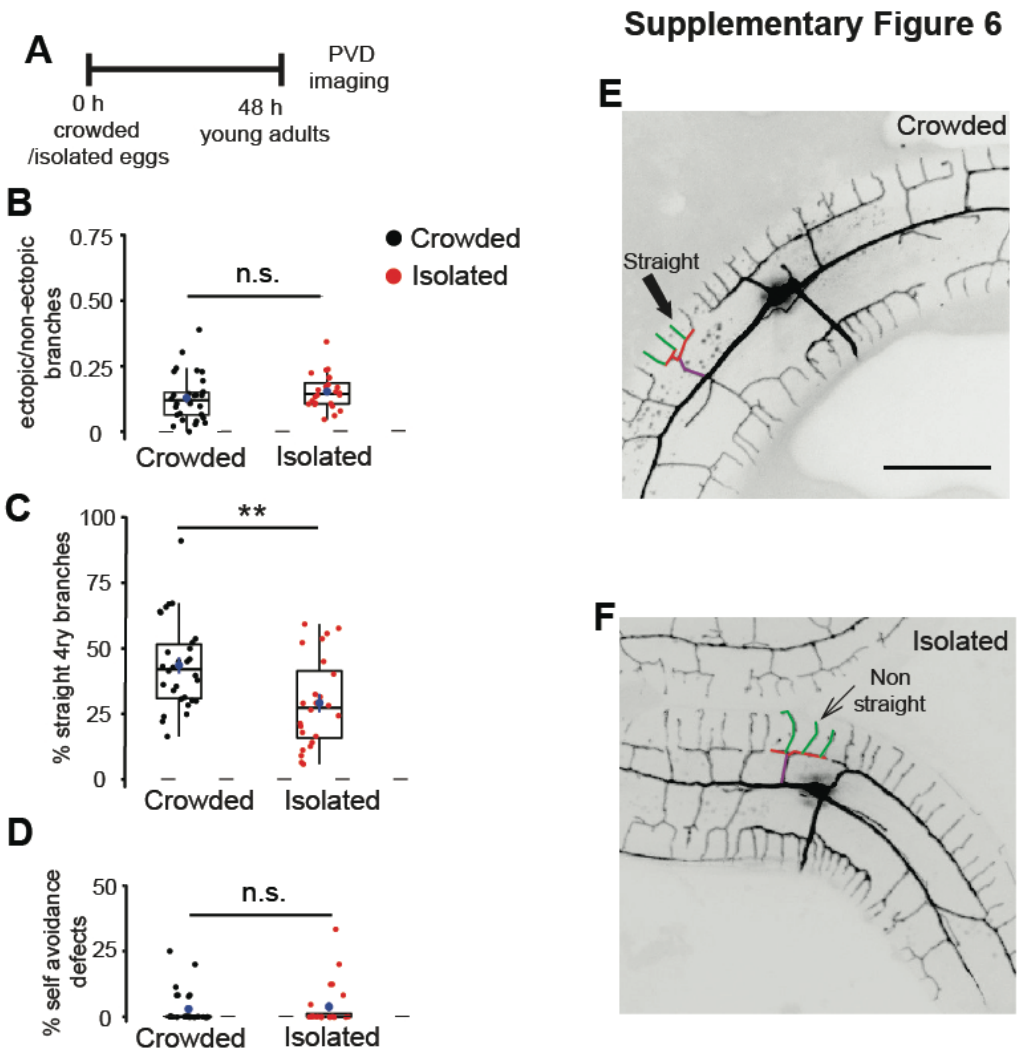

833 **Supplementary Figure 6: Isolation of eggs for 48 h is sufficient to induce some**
834 **changes in the structure of the PVD's quaternary branches. (A)** Schematic protocol
835 for the isolation of WT eggs for 48 h, followed by PVD imaging. **(B)** Isolation of eggs for
836 48 h (resulted in young adult worms) did not affect the number of ectopic branches, it
837 **(C)** decreased the percentage of straight quaternary branching and **(D)** it did not affect
838 the percentage of self-avoidance defects (Crowded, n=30; Isolated, n=24). **(E, F)**
839 Representative pictures from the PVD for crowded worms and isolated eggs. Scale bar
840 for panel 'E' represents 50 µm. The mean ± s.e.m. are shown in blue. Box plot with
841 hinge for the first and third quartile. The median is represented by the thick horizontal
842 black line and the whiskers are estimated calculation of the confidence interval 95%.
843 Mann Whitney test, ** p<0.01, n.s. not significant.

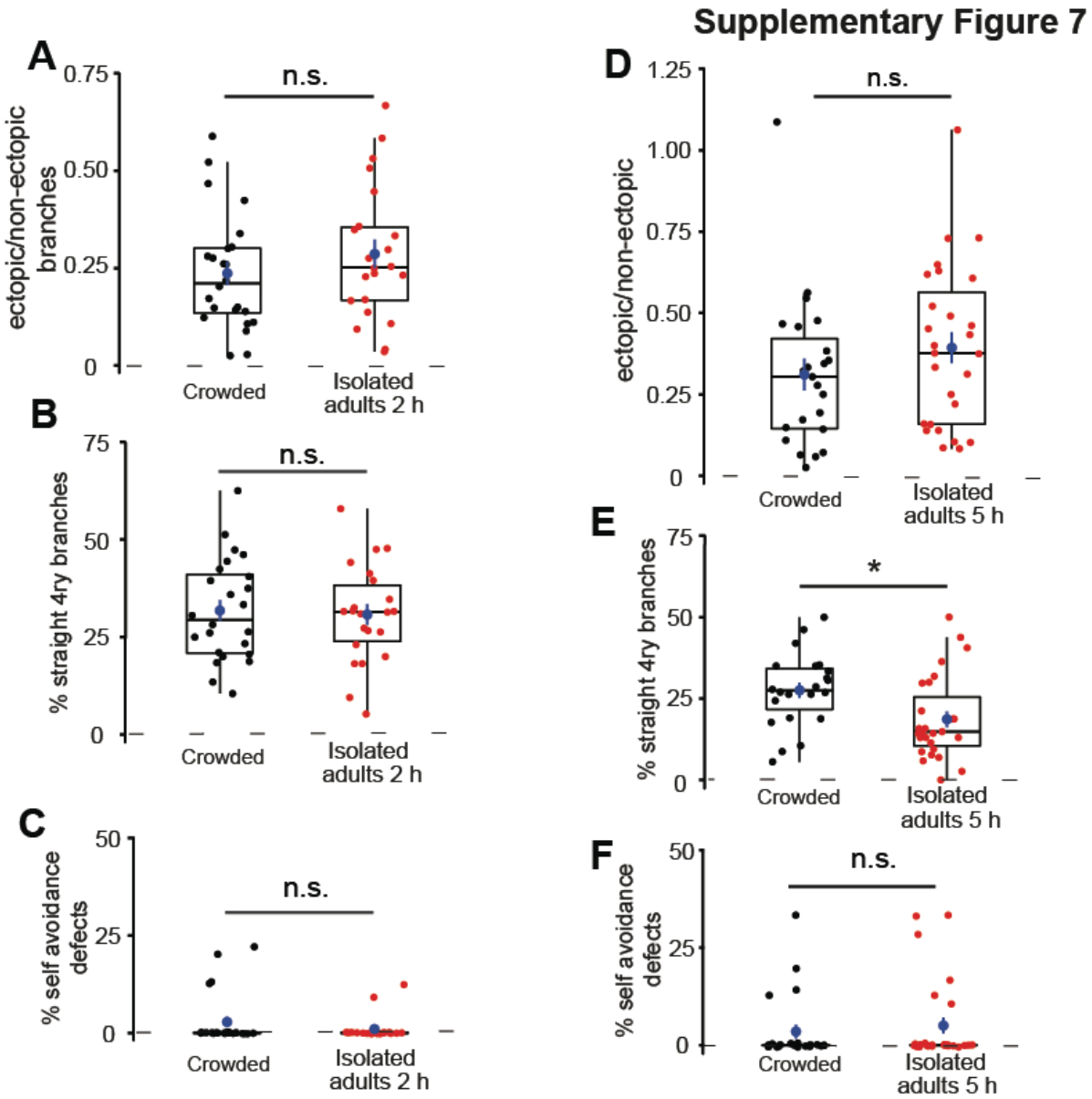

Supplementary Figure 7: Isolation of young adult worms for 5 h, but not 2 h, is sufficient to induce changes in the arborization pattern of the PVD. (A-C) Isolation of adult worms for 2 h was not sufficient to induce morphological changes on the PVD (Crowded, n=24; Isolated adults for 2 h, n=22)**. (D)** Isolation of adult worms for 5 h did not affect total ectopic branching, **(E)** it reduced the percentage of straight quaternary branching and **(F)** it did not affect the percentage of self-avoidance defects. (Crowded, n=24; Isolated adults for 5 h, n=27). The mean ± s.e.m. are shown in blue. Box plot with hinge for the first and third quartile. The median is represented by the thick horizontal black line and the whiskers are estimated calculation of the confidence interval 95%. Mann Whitney test, * $p<0.05$, n.s. not significant.

Supplementary Figure 8

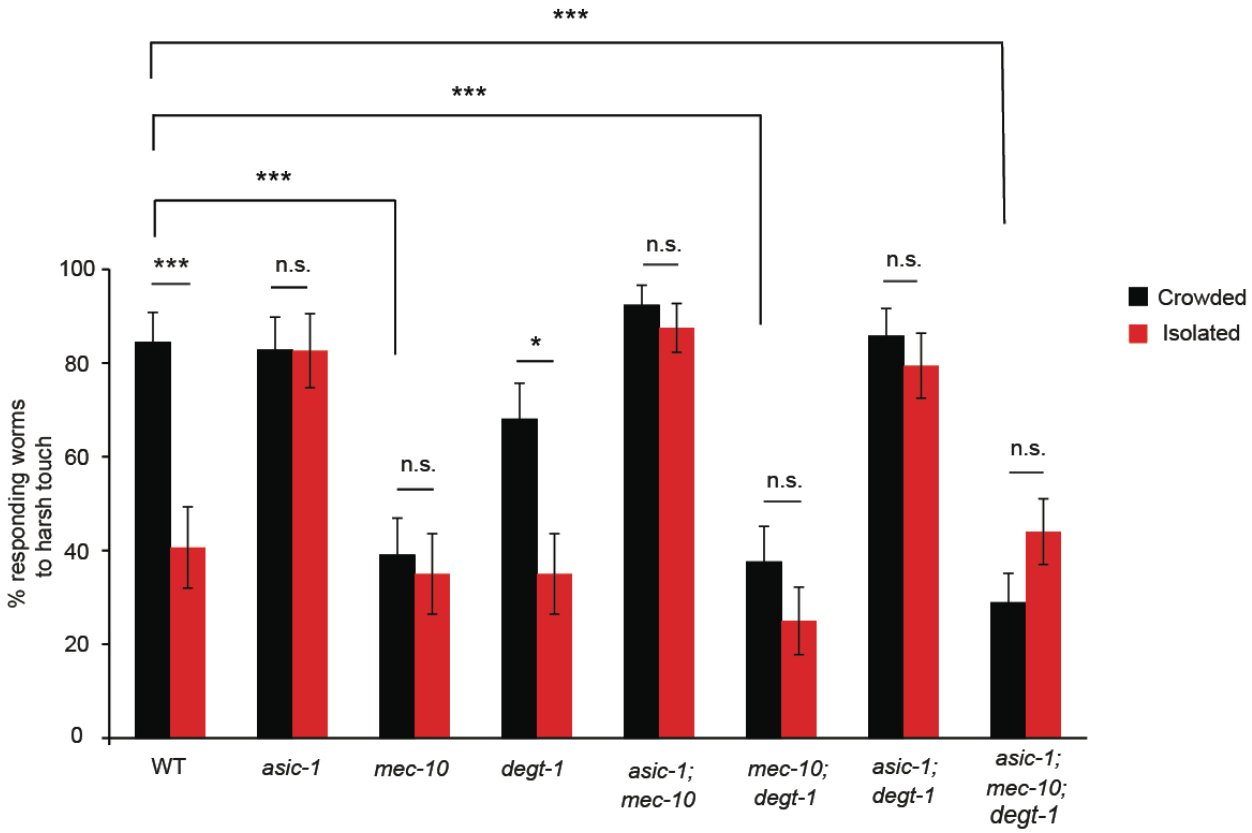

Supplementary Figure 8: The DEG/ENaC *asic-1* and *mec-10* mediate experience dependent behavioral plasticity following isolation. Posterior assay was performed for crowded and isolated WT and DEG-ENaC mutants, similar to the procedure described in Fig. 1b. Seven combinations of DEG-ENaC mutants were tested for the isolation effect on response. Isolated worms were compared to crowded worms from the same strain. N2 worms (The same set of worms as in Fig. 1C. Crowded, n=32; Isolated, n=32), *asic-1* (Crowded, n=46; Isolated, n=30), *mec-10* (Crowded, n=38; Isolated, n=31), *degt-1* (Crowded, n=37; Isolated, n=31), *asic-1;mec-10* (Crowded, n=20; Isolated, n=22), *mec-10*;*degt-1* (Crowded, n=40; Isolated, n=36), *asic-1*;*degt-1* (Crowded, n=35; Isolated, n=34), *asic-1*;*mec-10;degt-1* (Crowded, n=52; Isolated, n=50). The proportion (percentage) of responding worms ± the standard error of proportion. Fisher exact test, *p<0.05, *** p<0.001, n.s. not significant.

Supplementary Figure 9

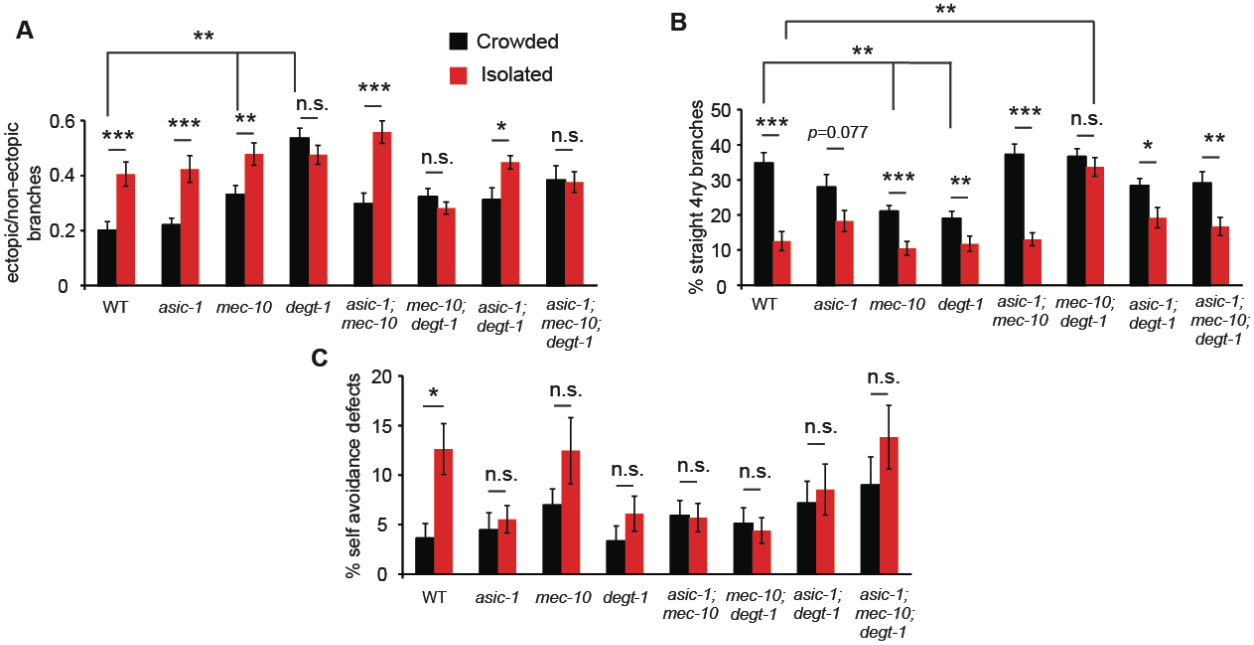

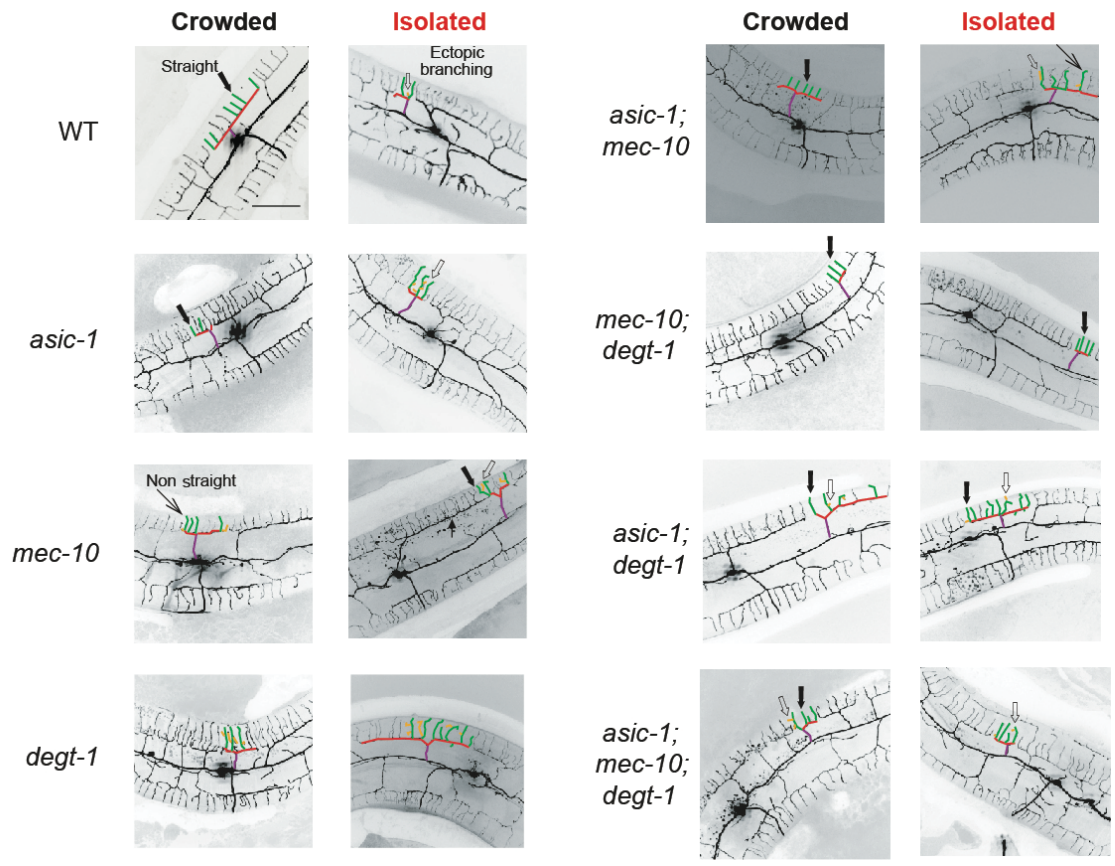

Supplementary Figure 9: The DEG-ENaCs, *mec-10* and *degt-1*, mediate mechanosensory dependent structural changes in the PVD.

Mutants of DEG-ENaC were isolated and were compared to crowded animals from the same strain, similar to the procedure described in Fig. 1b. **(A)** Three DEG-ENaC mutants: *degt-1, mec-10;degt-1*, and *asic-1*;*mec-10;degt-1* show no difference between crowded and isolated worms in terms of ectopic branching. In addition, crowded *mec-10 and degt-1* animals increased the number of ectopic branches compared to crowded WT worms while isolated *mec-10;degt-1* decreased it. **(B)** *mec-10;degt-1* mutants failed to decrease the percentage of straight quaternary branches, while *mec-10* and *degt-1* crowded decreased it, compared to the crowded WT animals. **(C)** The increase in self-avoidance defects following isolation is DEG-ENaC dependent. WT (The same set of worms as shown in Fig. 2B-D. Crowded, n=28; Isolated, n=26), *asic-1* (Crowded, n=22; Isolated, n=25), *mec-10* (Crowded, n=27; Isolated, n=21. The same set of worms as shown in Fig. 2B-D), *degt-1* (Crowded, n=28; Isolated, n=24), *asic-1;mec-10* (Crowded, n=30; Isolated, n=31), *mec-10*;*degt-1* (Crowded, n=26; Isolated, n=28), *asic-1*;*degt-1* (Crowded, n=23; Isolated, n=22), *asic-1*;*mec-10;degt-1* (Crowded, n=23; Isolated, n=21). **(D)** Representative pictures from the PVD for crowded and isolated worms of WT and seven different DEG-ENaC mutants. Scale bar for panel 'D' represents 50 µm. The mean ± s.e.m. are shown. Mann Whitney test, *p<0.05, ** p<0.01, *** p<0.001, n.s. not significant.

Supplementary movie captions

Movie S1: Localization pattern of MEC-10::mCherry in the PVD for crowded worms. MEC-10 is localized in moving vesicles, indicated by red arrow. Six z-stacks series (~60 optical slices for each) were taken around the CB every 3 minutes.

Movie S2: Localization pattern of MEC-10::mCherry in the PVD for crowded worms. MEC-10 is localized in moving vesicles, indicated by red arrow. Six z-stacks series (~60 optical slices for each) were taken around the CB every 2 minutes.